PTEP

Prog. Theor. Exp. Phys. **2025** 063B05 (35 pages)
DOI: 10.1093/ptep/ptaf080

Downloaded from https://academic.oup.com/ptep/article/2025/6/063B05/8140051 by SISSA - Scuola Internazionale Superiore di Studi Avanzati user on 15 June 2026

Entanglement Asymmetry in Conformal Field Theory and Holography

Francesco Benini [1,2,3,*], Victor Godet [1,2], and Amartya Harsh Singh [1,2]

[1] *SISSA, Via Bonomea 265, 34136 Trieste, Italy*
[2] *INFN, Sezione di Trieste, Via Valerio 2, 34127 Trieste, Italy*
[3] *ICTP, Strada Costiera 11, 34151 Trieste, Italy*

Received October 8, 2024; Revised March 5, 2025; Accepted May 20, 2025; Published May 21, 2025

Entanglement asymmetry is a measure of symmetry breaking in quantum subsystems, inspired by quantum information theory, particularly suited to study out-of-equilibrium states. We study the entanglement asymmetry of a class of excited "coherent states" in conformal quantum field theories with a $U(1)$ symmetry, employing Euclidean path-integral methods with topological symmetry defects and the replica formalism. We compute, at leading order in perturbation theory, the asymmetry for a variety of subsystems, including finite spherical subregions in flat space, in finite volume, and at positive temperature. We also study its Lorentzian time evolution, showcasing the dynamical restoration of the symmetry due to thermalization, as well as the presence of a quantum Mpemba effect. Our results are universal, and apply in any number of dimensions. We also show that the perturbative entanglement asymmetry is related to the Fisher information metric, which has a known holographic dual called the Hollands–Wald canonical energy, and that it is captured by the anti-de-Sitter bulk charge contained in the entanglement wedge.

Subject Index A56, A60, B21, B31, B87

1. Introduction

Symmetry and symmetry breaking are key concepts in quantum field theory (QFT). Indeed, often it is only through the lenses of symmetry breaking that we decode the complicated dynamics of many-body systems or strongly coupled QFTs. The traditional language to describe symmetry breaking is the Landau paradigm, i.e. the analysis of the expectation values of local order parameters. On the other hand, over the years, quantum information theory has been playing an increasingly important role in many-body systems and quantum field theory. For instance, in the context of QFT, quantum information can be used to derive monotonicity and positivity results [1–3]. In the context of AdS/CFT, quantum information allows us to understand the emergence of the bulk from conformal field theory (CFT) [4,5], to obtain the Page curve for toy models of evaporating black holes [6,7], and it appears to be well suited to study dynamics far from equilibrium [8].

Recently, a new quantum information observable—dubbed *entanglement asymmetry*—has been introduced in [9] to detect and quantify symmetry breaking in quantum subsystems, in particular out of equilibrium. It is a modification of entanglement entropy. Given a reduced density matrix ρ that describes a pure or mixed state as seen from within a subsystem A, and given a $U(1)$ action on the Hilbert space, Ares et al. [9] proposed to compare ρ with the average

*fbenini@sissa.it

© The Author(s) 2025. Published by Oxford University Press on behalf of the Physical Society of Japan.
This is an Open Access article distributed under the terms of the Creative Commons Attribution License (https://creativecommons.org/licenses/by/4.0/), which permits unrestricted reuse, distribution, and reproduction in any medium, provided the original work is properly cited.
Funded by SCOAP³

of ρ over the adjoint action of $U(1)$, which we call ρ_Q.[1] To be precise, the entanglement asymmetry ΔS is defined as the difference between the entanglement entropies of ρ and ρ_Q, and it turns out to be equivalent to a relative entropy:

$$\Delta S = \mathrm{Tr}(\rho \log \rho) - \mathrm{Tr}(\rho_Q \log \rho_Q) = S(\rho \parallel \rho_Q). \tag{1}$$

This is a good measure of symmetry breaking: by known properties of relative entropy, ΔS is nonnegative, and it vanishes if and only if the symmetry is unbroken in A.

Entanglement asymmetry was used in [9] to investigate a quantum version of the Mpemba effect [10–12] in spin chains. This is the phenomenon that excited symmetry-breaking states can relax and restore the symmetry faster than states in which the symmetry is less broken.[2] Such a counterintuitive behavior is only possible far from equilibrium. Subsequent works that studied entanglement asymmetry and the Mpemba effect include [14–29].

In this paper we are interested in computing entanglement asymmetry in quantum CFTs with a $U(1)$ symmetry in general dimensions d, with an eye towards holography. In QFT, entanglement entropy is known to suffer from UV divergences. For entanglement asymmetry instead, being a relative entropy, the divergences cancel out and we expect to obtain a well-defined observable. In CFTs the vacuum does not spontaneously break the symmetry, and thus we ought to consider some excited state. Here we study a class of "coherent states," partially motivated by holography [30–32], i.e.

$$|\Psi\rangle = e^{i\lambda V}|0\rangle, \tag{2}$$

obtained by acting on the vacuum with $e^{i\lambda V}$ in Euclidean time, where V is a primary local operator of charge 1.[3] We choose to work in a perturbative expansion in λ, and show that $\Delta S = \lambda^2 \Delta S^{(2)} + O(\lambda^4)$. We compute the leading contribution $\Delta S^{(2)}$ in three different ways.

(1) By first computing the Renyi asymmetries

$$\Delta S_n = \frac{1}{1-n}(\log \mathrm{Tr}\, \rho_Q^n - \log \mathrm{Tr}\, \rho^n) \tag{3}$$

using the replica method in [33–35], and then taking the limit $n \to 1$.

(2) By exploiting an integral representation for the leading perturbative contribution to relative entropy, also called the Fisher information [32,36].

(3) By computing the Renyi asymmetries in terms of correlation functions of V and $V^\dagger$ that include twist operators [34].

The result is a "universal expression" for the entanglement asymmetry that depends on the dimension Δ of V and on the location of its insertion in Euclidean space.

It turns out that both $\Delta S^{(2)}$ and $\Delta S_n^{(2)}$ behave as two-point functions. This allows us (for instance, as in [37]) to exploit conformal transformations to determine the entanglement asymmetry in a variety of geometries, for different choices of subsystem A: for the "Rindler" geometry in which A is an infinite half-space; for finite spherical subregions A in infinite volume as well as in finite volume on S^{d-1}; for spherical subregions on the hyperbolic plane $\mathbb{H}^{d-1}$ at finite temperature; for finite intervals on the real line at finite temperature in $d = 2$.

[1] In fact, this works for any group G: discrete, Abelian, and non-Abelian.

[2] Aristotle observed, some 2,300 years ago, that "to cool hot water quickly, begin by putting it in the sun." The quantum Mpemba effect has been observed experimentally in ion traps [13].

[3] Similar states have been studied in [21].

Downloaded from https://academic.oup.com/ptep/article/2025/6/063B05/8140051 by SISSA - Scuola Internazionale Superiore di Studi Avanzati user on 15 June 2026

Following [37,38], we are also able to use conformal transformations and analytic continuation to determine the time evolution of entanglement asymmetry, starting from a coherent state (that we regard as originating from a local quench). As expected from thermalization, the asymmetry of a subsystem decreases with time since the excited state relaxes. Interestingly, however, we observe that a universal quantum Mpemba effect takes place. It would be interesting to identify an underlying mechanism responsible for the Mpemba effect in CFTs (as done in [19] for integrable systems).

In the context of AdS/CFT, what is the holographic dual to entanglement asymmetry? At leading order in λ, entanglement asymmetry is Fisher information, and the latter has a known holographic dual [36] given by a suitable integral of the so-called symplectic flux in the entanglement wedge. We observe that such a quantity can be recast in a suggestive form:

$$\Delta S^{(2)} = 2\pi\, \partial_{\tau_0} \left(\int_{\widetilde{A}} \star F - \int_A \star F \right). \tag{4}$$

Here F is the field strength of the bulk gauge field dual to the $U(1)$ symmetry of the CFT, A is the chosen spatial subsystem at the boundary, $\widetilde{A}$ is the Ryu–Takayanagi surface (homologous to A) that describes entanglement entropy, while τ_0 is the boundary location of the insertion of V along the modular flow. This formula thus contains all the ingredients that we expect to be important in the holographic evaluation of entanglement asymmetry. We hope to be able to address the higher-order terms, and to obtain a better physical understanding of this formula, in future work.

2. Entanglement asymmetry

Let us review the definition of entanglement asymmetry proposed in [9].[4] Consider a quantum system that can be divided into two parts A and B in such a way that the Hilbert space factorizes: $\mathcal{H} = \mathcal{H}_A \otimes \mathcal{H}_B$. Given a (normalized) density matrix ρ_{tot}, which could represent a pure ($\rho_{\text{tot}} = |\psi\rangle\langle\psi|$) or a mixed state, one constructs the reduced density matrix on A, namely, $\rho = \text{Tr}_B\, \rho_{\text{tot}}$, and its entanglement entropy is given by the von Neumann entropy $S = -\,\text{Tr}(\rho \log \rho)$. Consider the case where there exists a charge operator Q that generates a $U(1)$ action on the Hilbert space,[5] and where the charge operator can be factorized as well:

$$Q = Q_A \otimes \mathbb{1}_B + \mathbb{1}_A \otimes Q_B. \tag{5}$$

If state ρ_{tot} is an eingenstate of Q, namely, $[\rho_{\text{tot}}, Q] = 0$ and thus the symmetry is unbroken, then $[\rho, Q_A] = 0$ and thus ρ takes a block-diagonal form in a basis of eigenspaces of Q_A. Then the entanglement entropy S can be resolved into the contributions $S(q)$ from each charge sector: this is called symmetry-resolved entanglement entropy [40–42]. On the other hand, if the symmetry is broken in subsystem A and thus $[\rho, Q_A] \neq 0$, one can quantify the amount of breaking in the following way. One constructs a projected reduced density matrix

$$\rho_Q = \sum_{q \in \mathbb{Z}} \Pi_q \rho \Pi_q, \tag{6}$$

where Π_q is the projector to the eigenspace of Q_A with charge q. This is essentially matrix ρ with all off-diagonal blocks set to zero. Quantity (6) can be recast in a more elegant form by

[4] Ma et al. [39] considered a very similar quantity, but for global states.

[5] In most cases, and in this paper too, the $U(1)$ action is a global symmetry of the quantum system. However, the Hamiltonian of the system does not enter into the definition of entanglement asymmetry and therefore one could consider $U(1)$ actions that are not symmetries, as, for instance, in [23].

Downloaded from https://academic.oup.com/ptep/article/2025/6/063B05/8140051 by SISSA - Scuola Internazionale Superiore di Studi Avanzati user on 15 June 2026

using the Fourier transform of the projector $\Pi_q = \int_0^{2\pi} d\alpha e^{i\alpha(Q_A - q)}/2\pi$; hence,

$$\rho_Q = \int_0^{2\pi} \frac{d\alpha}{2\pi} e^{-i\alpha Q_A} \rho e^{i\alpha Q_A}. \tag{7}$$

This is the average of ρ over the adjoint action of group $U(1)$, and it naturally generalizes to discrete as well as non-Abelian groups [16–18,23]. Note that ρ_Q is a density matrix, namely, it is Hermitian, semi-positive definite, and $\mathrm{Tr}\,\rho_Q = 1$. The entanglement asymmetry is defined as the difference between the entanglement entropies of ρ_Q and ρ [9]:

$$\Delta S = S[\rho_Q] - S[\rho] = \mathrm{Tr}(\rho \log \rho) - \mathrm{Tr}(\rho_Q \log \rho_Q). \tag{8}$$

One easily verifies that the entanglement asymmetry is equivalent to the relative entropy of ρ with respect to ρ_Q [39]:

$$\Delta S = \mathrm{Tr}[\rho(\log \rho - \log \rho_Q)] = S(\rho \,\|\, \rho_Q). \tag{9}$$

This makes ΔS a good measure of symmetry breaking. Indeed, as it follows from the properties of relative entropy, $\Delta S \geq 0$, and $\Delta S = 0$ if and only if $\rho = \rho_Q$, namely, if $[\rho, Q_A] = 0$ so that the symmetry is unbroken in A.

The entanglement asymmetry can be obtained from Renyi entanglement asymmetries using the replica trick [33,34]. The Renyi entanglement asymmetries are defined as

$$\Delta S_n = \frac{1}{1-n} \log \frac{\mathrm{Tr}(\rho_Q^n)}{\mathrm{Tr}(\rho^n)}. \tag{10}$$

The entanglement asymmetry is obtained from the limit $\Delta S = \lim_{n\to 1} \Delta S_n$. The moments $\mathrm{Tr}(\rho_Q^n)$ are easily obtained from Eq. (7). By a change of integration variables, they can be written as [9,39]

$$\mathrm{Tr}(\rho_Q^n) = \int_0^{2\pi} \frac{d\gamma_1 \cdots d\gamma_{n-1}}{(2\pi)^{n-1}} X_n(A, \gamma), \tag{11}$$

where we have defined the so-called charged moments

$$X_n(A, \gamma) = \mathrm{Tr}[\rho e^{i\gamma_1 Q_A} \rho e^{i\gamma_2 Q_A} \cdots \rho e^{i\gamma_{n-1} Q_A} \rho e^{-i(\gamma_1 + \cdots + \gamma_{n-1}) Q_A}]. \tag{12}$$

We could formally define $\gamma_n \equiv -(\gamma_1 + \cdots + \gamma_{n-1})$ so that $\sum_{j=1}^n \gamma_j = 0$. Thus, the charged moments implement all insertions of elements of $U(1)$ that multiply to the identity.

We are interested in studying entanglement asymmetry in quantum field theories, following [34]. In particular, we use the path integral over replicas in order to define and compute traces of density matrices. It is well known that the definition of entanglement entropy we presented is plagued by UV divergences when used in quantum field theory, as opposed to quantum mechanics. The situation improves for entanglement asymmetry (as it does in general for relative entropies) because the divergences cancel among the numerator and denominator of Eq. (10), at least as long as the symmetry breaking is spontaneous, or explicit but soft.

We consider states ρ_{tot} that have a Euclidean path-integral representation. In particular, given a spatial manifold $\mathcal{M}$, state ρ_{tot} is produced by the path integral on some Euclidean manifold, possibly with operator insertions, with a cut along a copy of $\mathcal{M}$. We call this geometry $\mathcal{G}$. Schematically, the matrix elements of such a state are

$$\langle \phi_- | \rho_{\mathrm{tot}} | \phi_+ \rangle = \frac{1}{Z} \int_{\substack{\text{geometry } \mathcal{G} \\ \varphi(0^-, \mathcal{M}) = \phi_- \\ \varphi(0^+, \mathcal{M}) = \phi_+}} \mathcal{D}\varphi (\cdots) e^{-S[\varphi]}. \tag{13}$$

Here $(t_{\mathrm{E}}, \mathcal{M})$ are Euclidean coordinates with t_{E} the Euclidean time and the cut at $t_{\mathrm{E}} = 0$, $\phi_\mp$ are Dirichlet boundary conditions for the fields, $(\cdots)$ are possible operator insertions, while Z is

Downloaded from https://academic.oup.com/ptep/article/2025/6/063B05/8140051 by SISSA - Scuola Internazionale Superiore di Studi Avanzati user on 15 June 2026

the partition function on $\mathcal{G}$ with the cut closed so as to guarantee that Tr $\rho_{\text{tot}} = 1$. The reduced density matrix ρ is obtained by partially closing the cut along B while keeping it open along $A \subset \mathcal{M}$. The moments of ρ are computed by

$$\mathrm{Tr}(\rho^n) = \frac{Z_n(A)}{Z^n}. \tag{14}$$

Here $Z_n(A)$ is the Euclidean path integral of the theory on a manifold $\mathcal{G}_n$ obtained by gluing together n identical copies of $\mathcal{G}$ (possibly with operator insertions) along the cut A, in such a way that the lower part of the cut on the nth copy is glued to the upper part of the cut on the $(n+1)$th copy. Then $Z \equiv Z_1(A)$ is the path integral on $\mathcal{G}$ (possibly with operator insertions) with the cut completely closed.

In order to compute the charged moments $X_n(A, \gamma)$ of ρ_Q, we need to insert operators $e^{i\gamma_j Q_A}$ into the trace [23]. In the path-integral description they are the topological codimension-one surfaces $U_\gamma[A]$, also called symmetry defects, that implement the $U(1)$ action on the Hilbert space [43], placed along the cut A. They are

$$U_\gamma[A] = \exp\left(i\gamma \int_A \star J\right) \quad \text{labeled by } \gamma \in [0, 2\pi) \cong U(1), \tag{15}$$

where J is the conserved $U(1)$ current operator, while "$\star$" is the Hodge star operation. Thus,

$$X_n(A, \gamma) = \frac{Z_n(A, \gamma)}{Z^n}. \tag{16}$$

Here $Z_n(A, \gamma)$ is the path integral on $\mathcal{G}_n$ with the insertion of topological symmetry defects $U_{\gamma_j}[A]$ along each of the gluings from one replica to the next. In the original geometry $\mathcal{G}$ it may appear that operator $U_\alpha[A]$ has a boundary along ∂A, and, in general, the boundaries of symmetry defect operators are *not* topological. However, on the covering geometry $\mathcal{G}_n$ there are n symmetry defects that join along ∂A and with parameters γ_j that sum to $0 \in U(1)$; therefore, in this case the junction of defects is topological as well.[6] Note that $Z_1(A, \gamma) = Z$.

Eventually, the path-integral formula for the Renyi asymmetries is

$$\Delta S_n = \frac{1}{1-n} \log \frac{[1/(2\pi)^{n-1}] \int d\vec{\gamma}\ Z_n(A, \gamma)}{Z_n(A)}, \tag{17}$$

where $d\vec{\gamma}$ is shorthand notation for $d\gamma_1 \cdots d\gamma_{n-1}$. Similar partition functions with topological defects were recently considered in [44] to study entanglement entropy in symmetric product orbifold CFTs.

There exists an alternative computational approach in which one considers n replicas of the theory, as opposed to n replicas of the Euclidean geometry. In this approach one computes the path integral of the theory in the presence of twist fields placed along ∂A that implement the gluing of one copy of the theory to the next as one crosses A [34]. In the context of entanglement asymmetry, the twist fields are dressed by the endpoints of a suitable symmetry defect placed along A [17,23]. We illustrate and utilize this approach in Appendix C.

[6]In the presence of an 't Hooft anomaly for the $U(1)$ symmetry, one may be worried that the path-integral definition of Renyi asymmetries is plagued by phase ambiguities: indeed, one needs to resolve the junction of n symmetry defects into a network of trivalent junctions, and different choices are related by nontrivial phases in the presence of an 't Hooft anomaly (we thank Giovanni Galati for raising this issue). In two dimensions each connected component of A is an interval with two ends. We insist that the resolution of the junction be specular on the two ends: in this way, if one changes the resolution, one obtains conjugate phases from the two ends and they cancel each other. In higher dimensions each connected component of A has a connected boundary, and we similarly insist that the resolution be "constant" along that boundary. We leave a more detailed study of possible effects of 't Hooft anomalies and higher-group structures on entanglement asymmetry for the future.

Downloaded from https://academic.oup.com/ptep/article/2025/6/063B05/8140051 by SISSA - Scuola Internazionale Superiore di Studi Avanzati user on 15 June 2026

$$\langle \phi_- |\, \rho \,| \phi_+ \rangle \quad = \quad \frac{1}{Z}$$

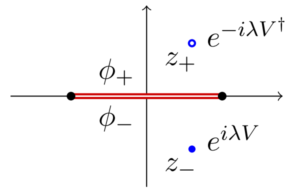

Fig. 1. Path-integral preparation of the reduced density matrix ρ for the excited coherent states $|\psi\rangle$ studied in this paper.

3. Asymmetry for CFTs in the Rindler geometry

We are interested in the computation of entanglement asymmetry in CFTs with a $U(1)$ symmetry.[7] Since the vacuum of a CFT does not exhibit spontaneous symmetry breaking, we should consider some excited state. In this paper we study a class of "coherent states" obtained by acting on the vacuum with a local operator $\mathcal{O}(z) = e^{i\lambda V(z)}$ inserted along Euclidean time.[8] Here V is a primary operator with fixed charge under Q that, for simplicity, we take to be 1, while λ is a small real parameter. The state is thus

$$|\psi\rangle = \mathcal{O}(z_-)\,|0\rangle = e^{i\lambda V(z_-)}\,|0\rangle, \qquad \rho_{\text{tot}} = |\psi\rangle\langle\psi| = e^{i\lambda V(z_-)}\,|0\rangle\langle 0|\, e^{-i\lambda V^\dagger(z_+)}. \tag{18}$$

Here z_- is the insertion point in the Euclidean past, while z_+ is its specular image under the inversion of Euclidean time. We give a graphical representation of the path integral in Fig. 1. Since operator $\mathcal{O}$ does not have definite charge, the state breaks the symmetry. This class of states is particularly natural from the point of view of holography, as we discuss in Section 5 below, and has already been studied in, for instance, [30–32].

Given a spatial manifold $\mathcal{M}$, the state is prepared by the Euclidean path integral on $\mathbb{R} \times \mathcal{M}$ (where the first factor is Euclidean time t_{E}) with a cut at $t_{\mathrm{E}} = 0$, the insertion of $\mathcal{O}(z_-)$ at a point z_- with $t_{\mathrm{E}} < 0$, and the insertion of $\mathcal{O}^\dagger(z_+)$, where z_+ is the point obtained from z_- by $t_{\mathrm{E}} \mapsto -t_{\mathrm{E}}$. We can then write the Renyi asymmetry (17) in terms of correlation functions:

$$\Delta S_n = \frac{1}{1-n} \log \frac{[1/(2\pi)^{n-1}] \int d\vec{\gamma}\ \langle \mathcal{O}_1 \mathcal{O}_1^\dagger \mathcal{L}_{\gamma_1} \cdots \mathcal{O}_n \mathcal{O}_n^\dagger \mathcal{L}_{\gamma_n} \rangle_{\mathcal{G}_n}}{\langle \mathcal{O}_1 \mathcal{O}_1^\dagger \cdots \mathcal{O}_n \mathcal{O}_n^\dagger \rangle_{\mathcal{G}_n}}. \tag{19}$$

Here $\mathcal{O}_j \equiv \mathcal{O}(z_{j-})$ is the operator inserted in the jth replica, while $\mathcal{L}_{\gamma_j}$ is the topological symmetry defects placed along the gluing from the jth to the $(j+1)$th replica. See also [21] where some Renyi asymmetries were discussed as correlation functions.

In this paper we content ourselves with computing the entanglement asymmetry at leading order in a perturbative expansion at small λ, i.e. in a limit in which the symmetry is only slightly broken. Calling Δ the dimension of the primary V, note that λ has dimensions of length$^\Delta$ and thus we study a limit in which λ is small compared to the Euclidean distance between the insertion point z_- and the cut A. In the denominator of Eq. (19) we find that

$$\langle \mathcal{O}_1 \mathcal{O}_1^\dagger \cdots \mathcal{O}_n \mathcal{O}_n^\dagger \rangle_{\mathcal{G}_n} = 1 + \lambda^2 \sum_{j,k} \langle V(z_{j-})\, V^\dagger(z_{k+}) \rangle_{\mathcal{G}_n} + O(\lambda^4). \tag{20}$$

[7] Entanglement asymmetry in CFTs in which the symmetry is explicitly broken has been studied in [23].

[8] More precisely, one should define $\mathcal{O}$ as a smeared operator $\mathcal{O} = e^{i\int d^d z\, \lambda(z)\, V(z)}$ obtained by integrating $V(z)$ on a region of spacetime in the Euclidean past. The resulting excited coherent state is $|\psi\rangle = e^{i\int d^d z\, \lambda(z)\, V(z)}|0\rangle$. This construction parallels the holographic setup discussed in Section 5 below. As the smearing function $\lambda(z)$ is concentrated on a smaller and smaller support, limiting to a Dirac delta function, operator $\mathcal{O}$ develops divergences. There are no divergences, however, at linear order in λ and, therefore, with some abuse, we keep using the notation $\mathcal{O}(z) = e^{i\lambda V(z)}$ for $\mathcal{O}$, with the above understanding in mind.

Downloaded from https://academic.oup.com/ptep/article/2025/6/063B05/8140051 by SISSA - Scuola Internazionale Superiore di Studi Avanzati user on 15 June 2026

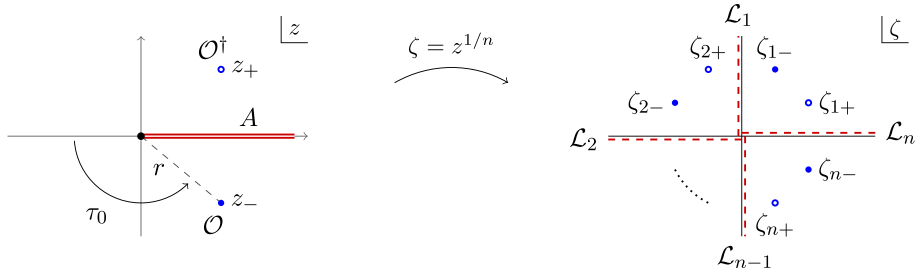

Fig. 2. Left: physical z plane of the Rindler geometry, with insertions of $\mathcal{O}$ at $z_- = r\,e^{-i(\pi-\tau_0)}$ and $\mathcal{O}^\dagger$ at $z_+ = z_-^*$. Right: covering ζ plane, in the case $n = 4$. The conformal map is $\zeta = z^{1/n}$.

Note that there are no terms with odd powers of λ because of charge conservation in the vacuum. Besides, at order λ^2 we never pick up the product of two V's or two $V^\dagger$'s at the same point and therefore we do not have to worry about divergences. In the numerator of Eq. (19) we have a correlator in the presence of the symmetry defects $\mathcal{L}_{\gamma_j}$. Since they are topological, we can swipe them through the replicas until they are all moved to the same sheet, and then we can collapse them on top of each other. Since the parameters sum up to zero, they disappear. However, when they cross a local operator, the correlator picks up a phase. We thus find that

$$\langle \mathcal{O}_1\mathcal{O}_1^\dagger\mathcal{L}_{\gamma_1}\cdots\mathcal{O}_n\mathcal{O}_n^\dagger\mathcal{L}_{\gamma_n}\rangle_{\mathcal{G}_n} = 1 + \lambda^2\sum_{j,k} e^{i\theta_{jk}}\langle V(z_{j-})\,V^\dagger(z_{k+})\rangle_{\mathcal{G}_n} + O(\lambda^4), \tag{21}$$

where $\theta_{jk} = \sum_{i=j}^{k-1}\gamma_i$ if $k > j$, or $\theta_{jk} = -\sum_{i=k}^{j-1}\gamma_i$ if $k < j$, or $\theta_{jk} = 0$ if $j = k$. Once we integrate in $d\vec{\gamma}$, all terms in the summation with a nontrivial phase are projected out, and therefore, for $j = k$, the summation reduces to

$$\frac{1}{(2\pi)^{n-1}}\int d\vec{\gamma}\,\langle \mathcal{O}_1\mathcal{O}_1^\dagger\mathcal{L}_{\gamma_1}\cdots\mathcal{O}_n\mathcal{O}_n^\dagger\mathcal{L}_{\gamma_n}\rangle_{\mathcal{G}_n} = 1 + \lambda^2\sum_j\langle V(z_{j-})V^\dagger(z_{j+})\rangle_{\mathcal{G}_n} + O(\lambda^4). \tag{22}$$

In other words, the integral projects to covering geometries in which the total charge vanishes copy by copy, not just globally in the union of copies. From Eq. (19) we eventually obtain

$$\Delta S_n = \frac{\lambda^2}{n-1}\sum_{j\neq k}^{n}\langle V(z_{j-})V^\dagger(z_{k+})\rangle_{\mathcal{G}_n} + O(\lambda^4). \tag{23}$$

This gives the leading perturbative contribution to the Renyi asymmetries.

3.1. *Two-dimensional CFTs and replicas*

Two-point functions on the replicated geometries $\mathcal{G}_n$ are nontrivial because the branching loci ∂A create curvature singularities. The two-dimensional case is special because, in certain cases, the singularities can be removed by a conformal transformation. We thus consider a 2D CFT, and the case in which A is the semi-infinite line to the right of the origin. Using a complex coordinate $z = z_2 + iz_1$ (where z_1 is Euclidean time and z_2 is space), we take $A = \{z \in \mathbb{R}_+\}$. We call this case the *Rindler geometry*, as in the left panel of Fig. 2 (we consider other geometries in Section 4 below). We can then compute correlators on $\mathcal{G}_n$ by exploiting a conformal covering map $\zeta = z^{1/n}$. Two-point functions transform as

$$\langle V(z_{j-})V^\dagger(z_{k+})\rangle_{\mathcal{G}_n} = \left|\frac{d\zeta}{dz}(\zeta_{j-})\frac{d\zeta}{dz}(\zeta_{k+})\right|^\Delta \langle V(\zeta_{j-})V^\dagger(\zeta_{k+})\rangle_{\mathbb{C}}, \tag{24}$$

where Δ is the dimension of V. We parametrize the insertion points $z_\pm$ as

$$z_- = re^{-i(\pi-\tau_0)}, \qquad z_+ = re^{i(\pi-\tau_0)}, \qquad r > 0,\ 0 < \tau_0 < \pi. \tag{25}$$

Downloaded from https://academic.oup.com/ptep/article/2025/6/063B05/8140051 by SISSA - Scuola Internazionale Superiore di Studi Avanzati user on 15 June 2026

On the covering ζ plane we take

$$\zeta_{j-} = r^{1/n} e^{i[2\pi(j-1/2)+\tau_0]/n}, \qquad \zeta_{j+} = r^{1/n} e^{i[2\pi(j-1/2)-\tau_0]/n}. \tag{26}$$

The twist lines $\mathcal{L}_j$ (before being removed) run along the semi-infinite lines with $\arg(\zeta) = 2\pi j/n$, as depicted in the right panel of Fig. 2. The two-point functions on the covering geometries $\mathcal{G}_n$ are

$$\langle V(z_{j-})V^\dagger(z_{k+})\rangle_{\mathcal{G}_n} = \frac{1}{n^{2\Delta} r^{2\Delta(n-1)/n} |\zeta_{j-} - \zeta_{k+}|^{2\Delta}}. \tag{27}$$

Writing the Renyi asymmetry as $\Delta S_n = \lambda^2 \Delta S_n^{(2)} + O(\lambda^4)$, the leading term from Eq. (23) is

$$\Delta S_n^{(2)} = \frac{n^{-2\Delta}}{n-1} \frac{1}{r^{2\Delta}} \sum_{j \neq k}^{n} \frac{1}{|2\sin\{[\tau_0 + (j-k)\pi]/n\}|^{2\Delta}}. \tag{28}$$

In order to compute the leading contribution $\Delta S^{(2)}$ to the entanglement asymmetry, we need to analytically continue Eq. (28) to complex values of n and then take the limit $n \to 1$. This means that we need to perform the sum explicitly. We were able to do that only for some integer values of 2Δ, using the Mellin transform

$$\frac{1}{\sin(\pi x)} = \frac{1}{\pi} \int_{\mathbb{R}} ds \frac{e^{sx}}{1+e^s} \quad \text{for } 0 < \mathbb{R}\mathrm{e}(x) < 1. \tag{29}$$

In Appendix A we perform the computation for $\Delta = \frac{1}{2}, 1, \frac{3}{2}, 2$. For instance, the Renyi asymmetry of the Rindler geometry takes the form

$$\Delta S_n^{(2)} = \frac{1}{4r^2} \frac{n}{n-1} \left(\frac{1}{\sin^2(\tau_0)} - \frac{1}{n^2 \sin^2(\tau_0/n)} \right) \quad \text{for } \Delta = 1; \tag{30}$$

therefore, the entanglement asymmetry is

$$\Delta S^{(2)}_{\text{Rindler}} = \frac{1}{2r^2 \sin^2(\tau_0)} \left(1 - \frac{\tau_0}{\tan(\tau_0)} \right) \quad \text{for } \Delta = 1. \tag{31}$$

In the next section we determine $\Delta S^{(2)}_{\text{Rindler}}$ for all $\Delta \in \mathbb{R}_+$.

3.2. *Asymmetry as relative entropy*

We can make progress in the computation of the leading contribution to the entanglement asymmetry of coherent states in a perturbative expansion in λ—in general dimension d—by using the fact that entanglement asymmetry is a relative entropy.

Given two density matrices ρ_0, ρ_1, their relative entropy is defined as

$$S(\rho_1 \,\|\, \rho_0) = \mathrm{Tr}(\rho_1 \log \rho_1) - \mathrm{Tr}(\rho_1 \log \rho_0). \tag{32}$$

Consider a continuous family $\rho(\lambda) = \rho_0 + \lambda\, \delta\rho + O(\lambda^2)$, normalized so that $\mathrm{Tr}\, \rho(\lambda) = 1$. Then, the relative entropy $S\big(\rho(\lambda) \,\|\, \rho_0\big)$ starts at second order in λ and at that order it is given by

$$\frac{1}{2} \frac{d^2}{d\lambda^2} S(\rho(\lambda) \,\|\, \rho_0) = F(\delta\rho, \delta\rho)_{\rho_0}, \tag{33}$$

where the quantity $F(\delta\rho_1, \delta\rho_2)_{\rho_0}$ is symmetric in its arguments and is called the Fisher information metric around ρ_0. There exists an integral formula for it (see, e.g. Appendix B of [32]):

$$F(\delta\rho_1, \delta\rho_2)_{\rho_0} = \frac{1}{4} \int_{-\infty}^{\infty} \frac{ds}{1+\cosh(s)} \mathrm{Tr}[\delta\rho_1 \rho_0^{-1/2 - is/2\pi} \delta\rho_2 \rho_0^{-1/2 + is/2\pi}]. \tag{34}$$

This formula is valid even if $\rho(\lambda)$ is not Hermitian, as long as it is normalized.

In our setup the reduced density matrix ρ is

$$\rho = \sigma + \lambda \sigma (iV - iV^\dagger) + O(\lambda^2), \tag{35}$$

Downloaded from https://academic.oup.com/ptep/article/2025/6/063B05/8140051 by SISSA - Scuola Internazionale Superiore di Studi Avanzati user on 15 June 2026

where $\sigma = \mathrm{Tr}_B |0\rangle\langle 0|$ is the reduced density matrix of the vacuum. Since the vacuum does not break the symmetry while $\sum_q \Pi_q \sigma V \Pi_q = 0$, we find that the projection ρ_Q differs from the vacuum only at second order in λ: $\rho_Q = \sigma + O(\lambda^2)$. We already noted that the entanglement asymmetry can be written as a relative entropy $\Delta S = S(\rho \,\|\, \rho_Q)$. Again, using the fact that σ commutes with Q_A, we can also write the asymmetry as $\Delta S = S(\rho \,\|\, \sigma) - S(\rho_Q \,\|\, \sigma)$. Since ρ_Q is equal to σ at first order in λ, the second term does not contribute at leading order. We thus obtain

$$\Delta S = \lambda^2 S^{(2)}(\rho \,\|\, \sigma) + O(\lambda^4). \tag{36}$$

We apply this formula to the Rindler geometry in $d \geq 2$ dimensions. The spatial slice is $\mathbb{R}^{d-1}$, subsystem A is a half-space, and the entangling surface ∂A is a $(d-2)$-dimensional plane. We use a complex coordinate z for the spatial direction orthogonal to the entangling surface and the Euclidean time direction, and y_i for the other coordinates (if any). The state is obtained from the vacuum with the insertion of $\mathcal{O} = e^{i\lambda V}$ at z_- and $\mathcal{O}^\dagger = e^{-i\lambda V^\dagger}$ at $z_+ = z_-^*$, both on the plane $y_i = 0$. We could more generally consider insertions at two generic points, not necessarily related by complex conjugation.[9] We will be interested in the case in which

$$z_- = re^{-i(\pi - \tau_-)} = re^{i\theta_-}, \qquad z_+ = re^{i(\pi - \tau_+)} = re^{i\theta_+}. \tag{37}$$

The reduced density matrix σ of the vacuum in the Rindler geometry is special because its modular Hamiltonian K defined by $\sigma = e^{-K}$ is local and geometric: it generates a counterclockwise rotation of the complex coordinate z around the entangling surface. We can thus write state ρ as

$$\begin{aligned}
\rho &= e^{-(1-\theta_-/2\pi)K} e^{i\lambda V} e^{-(\theta_- - \theta_+)K/2\pi} e^{-i\lambda V^\dagger} e^{-\theta_+ K/2\pi} \\
&= \sigma + i\lambda \sigma e^{\theta_- K/2\pi} V e^{-\theta_- K/2\pi} - i\lambda \sigma e^{\theta_+ K/2\pi} V^\dagger e^{-\theta_+ K/2\pi} + O(\lambda^2) \\
&= \sigma + i\lambda \sigma V(z_-) - i\lambda \sigma V^\dagger(z_+) + O(\lambda^2),
\end{aligned} \tag{38}$$

as already written in Eq. (35). To this state, we apply Eqs. (33)–(34). Taking into account charge conservation, we obtain two terms that are however equal using the change of variable $s \to -s$ and the cyclicity of the trace:

$$\Delta S^{(2)}_{\text{Rindler}} = \frac{1}{2} \int \frac{ds}{1 + \cosh(s)} \,\mathrm{Tr}[\sigma V^\dagger(z_+) \sigma^{-1/2 - is/2\pi} \sigma V(z_-) \sigma^{-1/2 + is/2\pi}]. \tag{39}$$

Shifting the integration contour as $s \to s + \pi i(1 - \varepsilon)$, where ε is an infinitesimal positive quantity that specifies a contour prescription, the integral is recast as

$$\Delta S^{(2)}_{\text{Rindler}} = -\frac{1}{4} \int \frac{ds}{\sinh^2(s/2 - i\varepsilon)} \,\mathrm{Tr}[\sigma \sigma^{-is/2\pi} V(z_-) \sigma^{is/2\pi} V^\dagger(z_+)]. \tag{40}$$

The trace contains operators time ordered with respect to modular time and is thus a two-point function. With $s = 0$, if we take two generic ordered points $z_j = e^{u_j + i\theta_j}$, we have

$$\begin{aligned}
\mathrm{Tr}[\sigma V(z_1) V^\dagger(z_2)] &= \langle V(z_1) V^\dagger(z_2) \rangle \\
&= \frac{1}{|z_1 - z_2|^{2\Delta}} \\
&= \frac{1}{\{2e^{u_1 + u_2}[\cosh(u_1 - u_2) - \cos(\theta_1 - \theta_2)]\}^\Delta} \\
&\equiv G_\Delta(u_1, \theta_1, u_2, \theta_2).
\end{aligned} \tag{41}$$

[9] In this case the Euclidean path integral prepares a non-Hermitian matrix.

Downloaded from https://academic.oup.com/ptep/article/2025/6/063B05/8140051 by SISSA - Scuola Internazionale Superiore di Studi Avanzati user on 15 June 2026

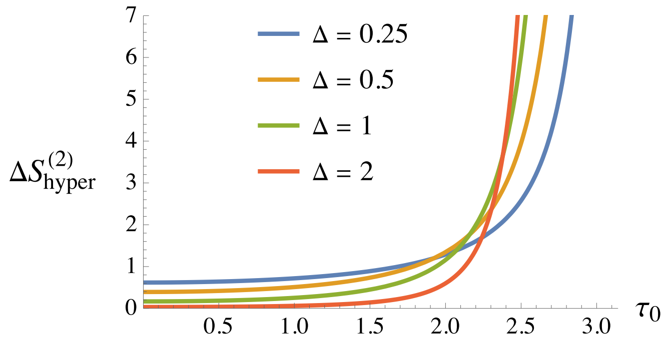

Fig. 3. The function $I_\Delta[\tan(\tau_0/2)]$ that describes $\Delta S^{(2)}_{\text{Rindler}}$ and $\Delta S^{(2)}_{\text{hyper}}$, plotted for different values of Δ as a function of $\tau_0 \in [0, \pi)$.

Since $V(z_-) = e^{\theta_- K/2\pi} V(r, 0) e^{-\theta_- K/2\pi}$, we see that $\sigma^{-is/2\pi} V(z_-) \sigma^{is/2\pi}$ has the net effect of shifting $\theta_- \to \theta_- + is$. The trace in Eq. (40) is then $G_\Delta(u, \theta_- + is, u, \theta_+) = G_\Delta(u, \pi + \tau_- + is, u, \pi - \tau_+)$ in terms of our parametrization. We obtain the formula

$$\Delta S^{(2)}_{\text{Rindler}} = -\int_{-\infty}^{+\infty} \frac{ds}{4r^{2\Delta} \sinh^2(s/2 - i\varepsilon)[-4\sinh^2(s/2 - i\tau_0)]^\Delta}, \tag{42}$$

where $\tau_0 = \frac{1}{2}(\tau_+ + \tau_-)$.

As we describe in Appendix B, the integral in Eq. (42) can be analytically performed in terms of a hypergeometric function. Let us define the function[10]

$$I_\Delta(x) = \frac{\sqrt{\pi}\,\Gamma(\Delta+1)}{4^\Delta \Gamma(\Delta + 1/2)} \left(1 - (1 - x^2)\frac{\Delta}{\Delta + 1/2}\, {}_2F_1\!\left[1, \frac{1}{2} - \Delta, \frac{3}{2} + \Delta; -x^2\right]\right). \tag{43}$$

Then

$$\Delta S^{(2)}_{\text{Rindler}} = \frac{1}{r^{2\Delta}} I_\Delta\!\left[\tan\left(\frac{\tau_0}{2}\right)\right]. \tag{44}$$

The entanglement asymmetry of the Rindler geometry starts at a finite value for $\tau_0 = 0$ and increases monotonically with a divergence at $\tau_0 = \pi$ with the following behaviors:[11]

$$\lim_{\tau_0 \to 0} \Delta S^{(2)}_{\text{Rindler}} = \frac{\sqrt{\pi}\,\Gamma(\Delta+1)}{2(2r)^{2\Delta}\Gamma(\Delta + 3/2)}, \qquad \Delta S^{(2)}_{\text{Rindler}} \underset{\tau_0 \to \pi}{\sim} \frac{2\pi\Delta}{(2r)^{2\Delta} \sin^{2\Delta+1}(\tau_0)}. \tag{45}$$

This is illustrated in Fig. 3 where we plot the function $I_\Delta[\tan(\tau_0/2)]$ for different values of Δ. For semi-integer values of Δ, we found alternative expressions for Eq. (42) in terms of trigonometric functions. For $\Delta \in \frac{1}{2} + \mathbb{Z}_{\geq 0}$, we found the expressions

$$\Delta S^{(2)}_{\text{Rindler}} = \frac{\pi\Delta}{(4r)^{2\Delta}\cos^{2\Delta+1}(\tau_0/2)}\left[1 + \sum_{k=1}^{\Delta - 3/2} \frac{(\Delta - 1/2 - k)(\Delta - 3/2 + k)!}{k!\,(\Delta - 1/2)!} \cos^{2k}\left(\frac{\tau_0}{2}\right)\right]. \tag{46}$$

The summation is finite and contributes only for $\Delta \geq \frac{5}{2}$. For $\Delta \in \mathbb{Z}_{\geq 1}$, we found that

$$\Delta S^{(2)}_{\text{Rindler}} = \frac{2\Delta}{(2r)^{2\Delta}\sin^{2\Delta}(\tau_0)}\left[1 - \frac{\tau_0}{\tan(\tau_0)} - \sum_{k=1}^{\Delta-1} \frac{(2k-2)!!}{(2k+1)!!} \sin^{2k}(\tau_0)\right]. \tag{47}$$

The summation is finite and contributes only for $\Delta \geq 2$. These expressions match those we already found in $d = 2$ for $\Delta = \frac{1}{2}, 1, \frac{3}{2}, 2$ using the replica method (see Appendix A).

[10] Recall that ${}_2F_1(a, b, c; z) = \sum_{n=0}^{\infty}[(a)_n(b)_n/(c)_n](z^n/n!)$ and, in particular, ${}_2F_1(a, b, c; 0) = 1$. The analytic continuation for $|z| \geq 1$ has a branch cut from 1 to ∞ along the positive real axis.

[11] They follow from $\lim_{x\to 0} I_\Delta(x) = \sqrt{\pi}\,\Gamma(\Delta+1)/[2^{2\Delta+1}\Gamma(\Delta+3/2)]$ and $I_\Delta(x) \sim \pi\Delta x^{2\Delta+1}/16^\Delta$ for $x \to +\infty$.

Downloaded from https://academic.oup.com/ptep/article/2025/6/063B05/8140051 by SISSA - Scuola Internazionale Superiore di Studi Avanzati user on 15 June 2026

4. Other geometries, relaxation, and the Mpemba effect

For the class of states (18) and at leading order in λ, it is clear from Eq. (23) that both Renyi and entanglement asymmetries behave as two-point functions. This means that in a CFT we can exploit conformal transformations to determine the asymmetry in geometries other than the Rindler one.[12] In this section we compute the entanglement asymmetry of finite spherical regions A in arbitrary dimensions, both in infinite volume, in a finite spherical volume, and in the hyperbolic plane at finite temperature.[13]

By analytic continuation from Euclidean to Lorentzian time, we will also be able to compute the time evolution of entanglement asymmetry in those geometries. Thus, entanglement asymmetry can be used to study dynamics: starting with a state that explicitly breaks the symmetry (in our setup regarded as a local quench at $t = 0$) we can study the dynamical restoration of the symmetry as expected from thermalization. In the context of quantum spin chains, entanglement asymmetry was used in [9] and subsequent works to provide a quantitative framework to study the Mpemba effect [10–12]—the observation that states farther away from equilibrium can relax faster. We observe a similar effect for the coherent states in CFTs in general dimensions.

First of all, we can use the computation of Section 3.2 of the entanglement asymmetry (44) of a CFT$_d$ in the Rindler geometry to determine the asymmetry of a thermal state in hyperbolic space. We already introduced flat coordinates $\{z_1, z_2, y_{i=1,\dots,d-2}\}$ on $\mathbb{R}^d$, where z_1 is Euclidean time, so that subsystem A is the half-space $A = \{z_1 = 0, z_2 \geq 0\}$. We also introduced a complex coordinate

$$z = z_2 + iz_1 = re^{i\tau}, \tag{48}$$

so that the metric takes the form $ds^2_{\text{Rindler}} = dr^2 + r^2 d\tau^2 + dy^2_{1,\dots,d-2}$ with $\tau \cong \tau + 2\pi$. Without loss of generality, we took the insertions at $z_\pm$ with $y_i = 0$, as in Eq. (37). We now perform a conformal (Weyl) transformation to $S^1 \times \mathbb{H}^{d-1}$:

$$ds^2_{\text{hyper}} = d\tau^2 + \frac{dr^2 + dy^2_{1,\dots,d-2}}{r^2} = \frac{1}{r^2}\, ds^2_{\text{Rindler}}. \tag{49}$$

This maps subsystem A of the Rindler geometry to the whole hyperbolic space $\mathbb{H}^{d-1}$ at $\tau = 0$. Since entanglement asymmetry transforms as a two-point function, it follows that $\Delta S^{(2)}_{\text{hyper}} = r^{2\Delta}\Delta S^{(2)}_{\text{Rindler}}$ and, therefore,

$$\Delta S^{(2)}_{\text{hyper}} = I_\Delta\left[\tan\left(\frac{\tau_0}{2}\right)\right], \tag{50}$$

where $\tau_0 = \frac{1}{2}(\tau_- + \tau_+)$ and I_Δ is as in Eq. (43). This is the entanglement asymmetry of an excited thermal state (with inverse temperature $\beta = 2\pi$) on the hyperbolic plane. It depends only on τ_0 (related to the Euclidean time of the insertions with respect to the cut) and not on the location on the hyperbolic plane because of its SO$(d-1, 1)$ isometry.

It is convenient to rewrite the metric on the hyperbolic geometry as

$$ds^2_{\text{hyper}} = d\tau^2 + du^2 + \sinh^2(u)\, d\Omega^2_{d-2} = \frac{dz\, d\bar{z}}{|z|^2} + \frac{1}{4}\left|z - \frac{1}{z^*}\right|^2 d\Omega^2_{d-2}, \tag{51}$$

[12] This is the same as what was done in [34,35,37] for the entanglement entropy.

[13] In $d = 2$ dimensions, the hyperbolic plane at finite temperature is identical to the standard real line at finite temperature.

Downloaded from https://academic.oup.com/ptep/article/2025/6/063B05/8140051 by SISSA - Scuola Internazionale Superiore di Studi Avanzati user on 15 June 2026

where $z = e^{u+i\tau}$ is some other complex coordinate,[14] while $d\Omega_{d-2}^2$ is the angular metric on a unit sphere S^{d-2}. Note that in $d > 2$ we take $u \geq 0$ and so $|z| \geq 1$, while in $d = 2$ we can neglect $d\Omega_{d-2}^2$ but take $u \in \mathbb{R}$. We consider a conformal (holomorphic) transformation

$$z = f(w), \quad \text{where} \quad w = r + it_{\mathrm{E}} \tag{52}$$

and t_{E} is Euclidean time. The metric takes the form

$$ds^2_{\text{hyper}} = \left|\frac{f'(w)}{f(w)}\right|^2 \left[dw\, d\bar{w} + \frac{(|f|^2-1)^2}{4|f'|^2}\, d\Omega^2_{d-2}\right] \equiv \Omega^2\, ds^2_{\text{geom}}. \tag{53}$$

This allows us to obtain the asymmetry in other geometries. We will be interested in transformations such that the coefficient of $d\Omega_{d-2}^2$ is only a function of r and not of t_{E}. In any case, the conformal factor Ω and parameter x are given by

$$\Omega = \left|\frac{f'(w_-)}{f(w_-)}\right|, \qquad x \equiv \tan\left(\frac{\tau_0}{2}\right) = -i\,\frac{z_- + |z_-|}{z_- - |z_-|} = -i\,\frac{f(w_-) + |f(w_-)|}{f(w_-) - |f(w_-)|}. \tag{54}$$

We thus obtain the general formula

$$\Delta S^{(2)}_{\text{geom}} = \Omega^{2\Delta} I_\Delta(x). \tag{55}$$

4.1. *Asymmetry for a finite subregion*

The choice

$$z = f(w) = \frac{w+\ell}{\ell - w} \tag{56}$$

in Eq. (53) gives the flat metric $ds^2_{\text{geom}} = dt^2_{\mathrm{E}} + dr^2 + r^2 d\Omega^2_{d-2}$ on $\mathbb{R}^d$. In $d > 2$ dimensions, the preimage of the hyperbolic plane is the spherical region $A = \{t_{\mathrm{E}} = 0,\ r^2 \leq \ell^2\}$ of radius ℓ that we call a disk. In $d = 2$ it is convenient to take $r \in \mathbb{R}$ and then subsystem A is the finite interval $r \in [-\ell, \ell]$. Using Eqs. (54)–(55), we can thus compute the entanglement asymmetry of a finite spherical subregion. The conformal factor and variable x in this case read

$$\Omega = \frac{2\ell}{|w_-^2 - \ell^2|}, \qquad x = \frac{2\ell\, \mathbb{I}\mathrm{m}(w_-)}{\ell^2 - |w_-|^2 - |w_-^2 - \ell^2|}, \tag{57}$$

in terms of the insertion point w_-, and $\Delta S^{(2)}_{\text{disk}} = \Omega^{2\Delta} I_\Delta(x)$ according to Eq. (55).

These formulas simplify if we take the insertion point w_- to lie along the imaginary axis $\mathbb{R}\mathrm{e}(w) = 0$. This is a vertical line (along Euclidean time) that goes through the center of the disk. Let us set[15]

$$w_- = -i\eta \tag{58}$$

in terms of a real parameter $\eta \in \mathbb{R}_+$. Then

$$\Omega = \frac{2\ell}{\ell^2 + \eta^2} \quad \text{and} \quad x = \tan\left(\frac{\tau_0}{2}\right) = \frac{\ell}{\eta}. \tag{59}$$

We thus obtain the following compact expression for the entanglement asymmetry of a disk in infinite volume:

$$\Delta S^{(2)}_{\text{disk}} = \left(\frac{2\ell}{\ell^2 + \eta^2}\right)^{2\Delta} I_\Delta\left(\frac{\ell}{\eta}\right). \tag{60}$$

In Appendix C we perform a check of this result by computing it in two dimensions from a four-point function of V, $V^\dagger$ and two twist operators (as in [34]), instead of using geometric replicas. In Fig. 4 (left) we plot the behavior of $\Delta S^{(2)}_{\text{disk}}$ with ℓ for some values of the parameters.

[14] The coordinate change from Eq. (49) to (51) is $(1 + r^2 + \vec{y}^2)/2r = \cosh(u)$, $(1 - r^2 - \vec{y}^2)/2r = \sinh(u)\,\theta_{d-1}$, $y^j/r = \sinh(u)\,\theta_j$ for $j = 1, \ldots, d-2$, so that $\theta_{a=1,\ldots,d-1} \in S^{d-2}$ satisfy $\sum_a \theta_a^2 = 1$.

[15] This corresponds to $e^{i\tau_0} = (i\eta - \ell)/(i\eta + \ell)$.

Downloaded from https://academic.oup.com/ptep/article/2025/6/063B05/8140051 by SISSA - Scuola Internazionale Superiore di Studi Avanzati user on 15 June 2026

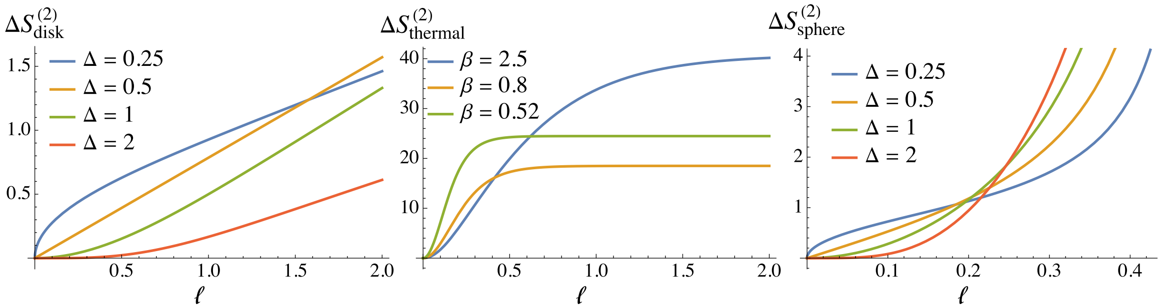

Fig. 4. Entanglement asymmetries in various geometries for insertions along the imaginary lines. Left: asymmetry $\Delta S^{(2)}_{\text{disk}}$ of a finite subregion as a function of ℓ for $\eta = 1$. Center: asymmetry $\Delta S^{(2)}_{\text{thermal}}$ at finite temperature β^{-1} as a function of ℓ for $\Delta = 1$ and $\eta = \frac{1}{4}$. Right: asymmetry $\Delta S^{(2)}_{\text{sphere}}$ in finite volume as a function of ℓ for $L = 1$ and $\eta = \frac{1}{3}$ (central line).

The expression in Eq. (60) has the following asymptotic behaviors:

$$\Delta S^{(2)}_{\text{disk}} \simeq \frac{\sqrt{\pi}\,\Gamma(\Delta+1)}{2\Gamma(\Delta+3/2)} \frac{\ell^{2\Delta}}{\eta^{4\Delta}} \quad \text{for } \ell \ll \eta, \qquad \Delta S^{(2)}_{\text{disk}} \simeq \frac{\pi\Delta}{4^{\Delta}} \frac{\ell}{\eta^{2\Delta+1}} \quad \text{for } \eta \ll \ell. \tag{61}$$

In particular, $\Delta S^{(2)}$ increases and diverges as ℓ for large intervals. We believe that this behavior will be corrected asymptotically by higher-order contributions to ΔS. Note also that $\Delta S^{(2)}$ is dimensionful, in accord with the fact that $\Delta S = \lambda^2 \Delta S^{(2)} + O(\lambda^4)$ and λ has dimensions of length$^{\Delta}$. A natural normalization (that we will use later) would be to fix λ in units of η^{Δ}.

4.2. *Asymmetry at finite temperature and in finite volume*

The choice

$$z = f(w) = \frac{\sinh[\pi(w+\ell)/\beta]}{\sinh[\pi(\ell - w)/\beta]}, \tag{62}$$

which implies the identification $w \cong w + i\beta$, when substituted into Eq. (53) gives

$$ds^2_{\text{geom}} = dt_{\text{E}}^2 + dr^2 + \frac{\beta^2}{4\pi^2} \sinh^2\left(\frac{2\pi r}{\beta}\right) d\Omega^2_{d-2}. \tag{63}$$

This is the metric on $S^1_\beta \times \mathbb{H}^{d-1}$, where the Euclidean time circle has radius β. In $d > 2$ dimensions we take $r \geq 0$ and the preimage of the hyperbolic plane is the spherical region $A = \{t_{\text{E}} = 0, r^2 \leq \ell^2\}$ inside $\mathbb{H}^{d-1}$. This geometry therefore describes an excited thermal state (with temperature β^{-1}) on the hyperbolic plane $\mathbb{H}^{d-1}$ (with curvature proportional to β^{-2}), reduced to a spherical subsystem A. Since the state lives on the hyperbolic plane, it does not originate from the standard thermal vacuum. On the other hand, in $d = 2$ dimensions we take $r \in \mathbb{R}$ and the geometry is just $S^1_\beta \times \mathbb{R}$, while subsystem A is the interval $r \in [-\ell, \ell]$: this is a finite subsystem in the standard thermal setup. The entanglement asymmetry is given by Eqs. (54)–(55).

For insertions along the imaginary axis $w_- = -i\eta$ (we take $0 < \eta < \beta/2$), namely, along the Euclidean circle that goes through the center of disk A, we find that

$$\Delta S^{(2)}_{\text{thermal}} = \left(\frac{2\pi\beta^{-1}\sinh(2\pi\ell/\beta)}{\cosh(2\pi\ell/\beta) - \cos(2\pi\eta/\beta)}\right)^{2\Delta} I_\Delta\left(\frac{\tanh(\pi\ell/\beta)}{\tan(\pi\eta/\beta)}\right). \tag{64}$$

We plot it in Fig. 4 (center) for some values of the parameters. In the limit $\beta \gg \ell, \eta$ we recover the entanglement asymmetry (60) of a disk in infinite volume. For $\ell \gg \beta$, we have

Downloaded from https://academic.oup.com/ptep/article/2025/6/063B05/8140051 by SISSA - Scuola Internazionale Superiore di Studi Avanzati user on 15 June 2026

$\tau_0 \simeq \pi(1-2\eta/\beta)$ and therefore the asymmetry asymptotes to a constant:

$$\Delta S^{(2)}_{\text{thermal}} \simeq (2\pi/\beta)^{2\Delta} I_\Delta[\cot(\pi\eta/\beta)] \quad \text{for } \ell \gg \beta. \tag{65}$$

This reproduces Eq. (50) for $\beta = 2\pi$.

The choice

$$z = f(w) = \frac{\sin[\pi(w+\ell)/L]}{\sin[\pi(\ell-w)/L]} \tag{66}$$

with $0 < \ell < L/2$ in Eq. (53) gives

$$ds^2_{\text{geom}} = dt^2_{\text{E}} + dr^2 + \frac{L^2}{4\pi^2}\sin\left(\frac{2\pi r}{L}\right)^2 d\Omega^2_{d-2}. \tag{67}$$

This is the metric on $\mathbb{R} \times S^{d-1}$ where the sphere has circumference L. Note that Eq. (66) implies the identification $w \cong w + L$. In $d > 2$ dimensions we take $0 \le r \le L/2$ and the preimage of the hyperbolic plane is the spherical region $A = \{t_{\text{E}} = 0, r^2 \le \ell^2\}$ inside the sphere S^{d-1}. In $d = 2$ we take $r \cong r + L$ and A is the interval $r \in [-\ell, \ell]$ inside this circle. This geometry allows us to evaluate the asymmetry of a spherical disk in finite volume. The general formula is Eqs. (54)–(55).

We consider two interesting cases in which the expressions simplify. One is of insertions along the imaginary axis $w_- = -i\eta$ that is the Euclidean time line through the center of the disk. We call this the central line, and we find that

$$\Delta S^{(2)}_{\text{sphere}} = \left(\frac{2\pi L^{-1}\sin(2\pi\ell/L)}{\cosh(2\pi\eta/L) - \cos(2\pi\ell/L)}\right)^{2\Delta} I_\Delta\left(\frac{\tan(\pi\ell/L)}{\tanh(\pi\eta/L)}\right). \tag{68}$$

We plot it in Fig. 4 (right) for some values of the parameters. Note that $2\pi\ell/L < \tau_0 < \pi$. For $L \gg \ell, \eta$, we recover asymmetry (60) of a disk in infinite volume. For $\ell \to L/2$ (i.e. if subspace A is the whole space), the asymmetry $\Delta S^{(2)}$ diverges; however, we believe that this is an artifact of the perturbative expansion. On the other hand, for $\eta \to \infty$, the asymmetry vanishes because the Euclidean time evolution projects the state to the ground state, which is symmetric.

The other case is of insertions along the axis $\mathbb{R}\text{e}(w) = L/2$ that we parametrize as $w_- = L/2 - i\eta$. This is the Euclidean time line that goes through the antipodal point on the sphere with respect to the center of the disk, and we call it the antipodal line. We find that

$$\Omega = \frac{2\pi L^{-1}\sin(2\pi\ell/L)}{\cosh(2\pi\eta/L) + \cos(2\pi\ell/L)}, \qquad x = \tan\left(\frac{\tau_0}{2}\right) = \tan(\pi\ell/L)\tanh(\pi\eta/L), \tag{69}$$

and $\Delta S^{(2)}_{\text{sphere}} = \Omega^{2\Delta} I_\Delta(x)$. In this case $0 < \tau_0 < 2\pi\ell/L$.

4.3. *Time dependence and relaxation*

As in [37,38], we can use conformal transformations and analytic continuation to obtain the time evolution of entanglement asymmetry, as follows. One first computes the entanglement asymmetry of a configuration in which the cut A is shifted by ξ along the Euclidean time direction, as in Fig 5. In our setup, this is equivalent to a geometry in which A is left untouched at $t_{\text{E}} = 0$, but the insertions are shifted as $\mathcal{O}(w_- - i\xi)$ and $\mathcal{O}^\dagger(w_-^* - i\xi)$. Since such a configuration is not specular with respect to the spatial slice of the cut at $t_{\text{E}} = 0$, the path integral prepares a "density matrix"

$$\rho_\xi = \text{Tr}_B(e^{-(\eta+\xi)H}\mathcal{O}|0\rangle\langle 0|\,\mathcal{O}^\dagger e^{-(\eta-\xi)H}) \tag{70}$$

(where $\eta = |\,\mathbb{I}\text{m}\, w_-|$), which, for real ξ, is not Hermitian. In order to compute the asymmetry of ρ_ξ in general, one needs to extend the evaluation of the integral in Eq. (40) (that computes

Downloaded from https://academic.oup.com/ptep/article/2025/6/063B05/8140051 by SISSA - Scuola Internazionale Superiore di Studi Avanzati user on 15 June 2026

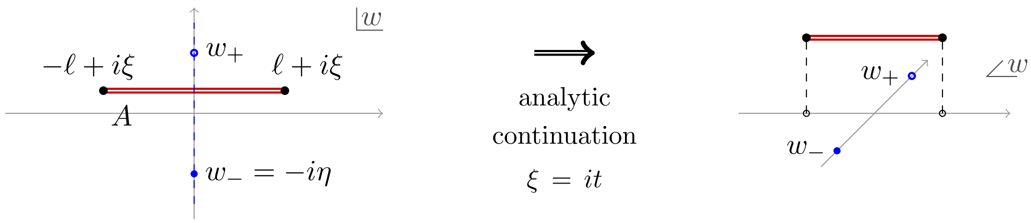

Fig. 5. The time evolution of entanglement asymmetry can be computed by first shifting the cut A along the Euclidean time direction by ξ, and then performing analytic continuation $\xi = it$ to Lorentzian time t.

the asymmetry in the Rindler geometry) to the case that $z_\pm$ have different absolute values. In the thermal hyperbolic geometry, this corresponds to having $\mathcal{O}, \mathcal{O}^\dagger$ inserted at different points on the hyperbolic plane. Then one takes the analytic continuation $\xi = it$, which produces the time-evolved Hermitian density matrix

$$\rho(t) = e^{-itH_A} \rho e^{itH_A}. \tag{71}$$

Now the configuration is specular with respect to the spatial slice, the cut is shifted in the Lorentzian time direction, and the path integral is performed along a Schwinger–Keldysh contour. This setup can be regarded as a local quench:[16] at $t = 0$ the system is in an excited state prepared by the Euclidean path integral, and for $t > 0$, it relaxes towards the vacuum.

In the special cases that the orbits of $w_- - i\xi$ and $w_+ - i\xi$ (as we vary ξ) have $|z_-| = |z_+|$ in the Rindler geometry (or, equivalently, $u_- = u_+$ in the thermal hyperbolic geometry), we can use Eq. (42). These special cases are precisely the "imaginary lines" we already discussed in the previous sections. Let us discuss the various cases separately.

4.3.1. *Finite spherical subregion.* We consider the geometry of Section 4.1 with a spherical subsystem $A = \{t_\mathrm{E} = 0, r^2 \leq \ell^2\}$ in $\mathbb{R}^d$ and insertions along the imaginary axis $\mathbb{R}\mathrm{e}(w) = 0$. With insertions at $w_- = -i(\eta + \xi)$ and $w_+ = i(\eta - \xi)$ we find that

$$\tan\left(\frac{\tau_-}{2}\right) = \frac{\ell}{\eta + \xi}, \qquad \tan\left(\frac{\tau_+}{2}\right) = \frac{\ell}{\eta - \xi}. \tag{72}$$

Including the conformal factors, the entanglement asymmetry takes the form

$$\Delta S^{(2)} = \left[\frac{4\ell^2}{[\ell^2 + (\eta + \tau)^2][\ell^2 + (\eta - \tau)^2]}\right]^\Delta I_\Delta\left[\tan^2\left(\frac{\tau_0}{2}\right)\right], \tag{73}$$

where $\tau_0 = \frac{1}{2}(\tau_- + \tau_+)$. We then perform the analytic continuation $\xi = it$ and obtain

$$\Delta S^{(2)}_{\text{quench}} = \left|\frac{2\ell}{\ell^2 + (\eta + it)^2}\right|^{2\Delta} I_\Delta(x), \tag{74}$$

where

$$x = \tan\left[\mathbb{R}\mathrm{e}\arctan\left(\frac{\ell}{\eta + it}\right)\right] = \frac{\ell^2 - \eta^2 - t^2 + \sqrt{(\ell^2 - \eta^2 - t^2)^2 + 4\ell^2\eta^2}}{2\ell\eta}. \tag{75}$$

Both the conformal factor Ω and x are as in Eq. (57) but evaluated at $w_- = t - i\eta$. This describes the time evolution of entanglement asymmetry after a local quench. We plot $\lambda^2 \Delta S^{(2)}_{\text{quench}}(t)$ for a choice of Δ, η and different values of ℓ in Fig. 6. Using a normalization of λ^2 so as to have

[16] We call the quench "local" (as opposed to "global") because it is localized in space and it produces an inhomogeneous state.

Downloaded from https://academic.oup.com/ptep/article/2025/6/063B05/8140051 by SISSA - Scuola Internazionale Superiore di Studi Avanzati user on 15 June 2026

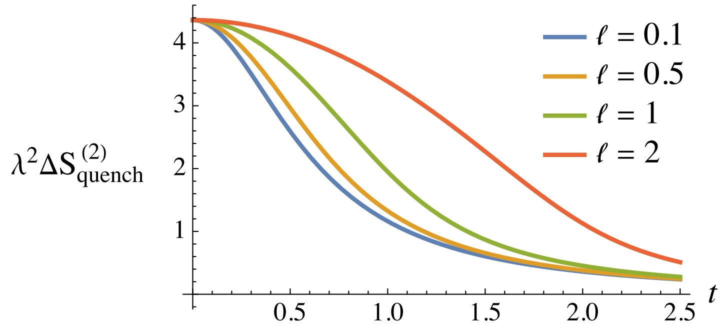

Fig. 6. Time evolution of the entanglement asymmetry $\lambda^2 \Delta S^{(2)}_{\text{quench}}(t)$ of a disk after a local quench for $\eta = 0.6$, $\Delta = 0.5$, and different values of the disk radius ℓ. We normalized $\lambda^2 \propto \ell^{-1}$ in order to have the same initial value. Note that larger subsystems thermalize more slowly.

the same initial value for the asymmetry, we see that larger subsystems thermalize more slowly. We explore other physical consequences of Eq. (74) in Section 4.4 below.

4.3.2. *Finite temperature.* For the finite-temperature geometry $S^1_\beta \times \mathbb{H}^{d-1}$ of Section 4.2 and insertions along the imaginary axis, proceeding as before we find that

$$\Delta S^{(2)}_{\text{T quench}} = \left| \frac{2\pi\beta^{-1} \sinh(2\pi\ell/\beta)}{\cosh(2\pi\ell/\beta) - \cos[2\pi(\eta + it)/\beta]} \right|^{2\Delta} I_\Delta(x) \tag{76}$$

with

$$x = \tan\left[\mathbb{R}\mathrm{e} \arctan\left(\frac{\tanh(\pi\ell/\beta)}{\tan[\pi(\eta + it)/\beta]} \right) \right]. \tag{77}$$

Parameter x can also be expressed as in Eq. (54) with $w_- = t - i\eta$.

4.3.3. *Finite volume.* For the geometry $\mathbb{R} \times S^{d-1}$ of Section 4.2 and insertions along the imaginary axis (that we called the central line), we find that

$$\Delta S^{(2)}_{\text{L quench}} = \left| \frac{2\pi L^{-1} \sin(2\pi\ell/L)}{\cosh[2\pi(\eta + it)/L] - \cos(2\pi\ell/L)} \right|^{2\Delta} I_\Delta(x) \tag{78}$$

with

$$x = \tan\left[\mathbb{R}\mathrm{e} \arctan\left(\frac{\tan(\pi\ell/L)}{\tanh[\pi(\eta + it)/L]} \right) \right]. \tag{79}$$

One can obtain a similar expression for insertions along the antipodal line. In both cases parameter x can also be expressed as in Eq. (54) with $w_- = t - i\eta$.

4.4. *Mpemba effect*

In this section we analyze some physical consequences of the time evolution of entanglement asymmetry. Before doing that, note that the primary operator V has dimensions of mass$^\Delta$, while λ has dimensions of length$^\Delta$. It is then more natural to parametrize

$$\lambda = \epsilon \eta^\Delta \tag{80}$$

in terms of a (small) dimensionless parameter ϵ. This is the normalization we will use in the rest of this section; hence, the entanglement asymmetry takes the form

$$\Delta S = \epsilon^2 \eta^{2\Delta} \Omega^{2\Delta} I_\Delta(x) + O(\epsilon^4) \tag{81}$$

at leading order in ϵ.

Downloaded from https://academic.oup.com/ptep/article/2025/6/063B05/8140051 by SISSA - Scuola Internazionale Superiore di Studi Avanzati user on 15 June 2026

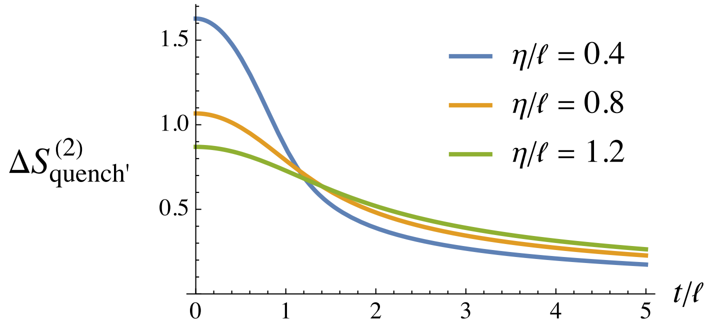

Fig. 7. Thermalization curves $\Delta S^{(2)}_{\text{quench}'}(t) \equiv \eta^{2\Delta} \Delta S^{(2)}_{\text{quench}}(t)$ for states created with different values of η at fixed $\Delta = 0.2$. We observe the Mbempa effect between any two such curves.

Let us first study the case of a finite subsystem in infinite volume given by Eq. (74). Since the conformal factor and parameter x behave as $\Omega \sim 2\ell/t^2$ and $x \sim \eta\ell/t^2$ for large t, at late times the asymmetry is controlled by the constant $I_\Delta(0)$ and, more precisely,

$$\Delta S \sim \epsilon^2 \frac{\sqrt{\pi}\,\Gamma(\Delta+1)}{2\Gamma(\Delta+3/2)} \left(\frac{\eta\ell}{t^2}\right)^{2\Delta} \quad \text{for } t \to \infty. \tag{82}$$

Defining a thermalization timescale t_* as the time at which ΔS gets reduced by a factor of e, we obtain

$$t_* = \sqrt{\eta\ell}\, e^{1/4\Delta}. \tag{83}$$

We see that thermalization is slower if we increase η, while it is faster if we increase the conformal dimension Δ. The two parameters η, Δ label the class of states we consider, and it is interesting to compare the thermalization of different states.

Consider two symmetry-breaking states ρ, ρ' and compare how fast they thermalize. How much these states break the symmetry is quantified by the initial value ΔS_0 of the asymmetry at $t = 0$. The speed at which they thermalize is quantified by the corresponding thermalization timescales t_* and t'_*. The Mpemba effect [10–12] occurs when, despite the symmetry being more broken, the thermalization timescale is shorter. This can be expressed using a quantity

$$m = \frac{\Delta S'_0 - \Delta S_0}{t'_* - t_*}. \tag{84}$$

If $m \geq 0$, the state starting at a higher ΔS_0 takes more time to equilibrate and there is no Mpemba effect. If $m < 0$, instead, that state relaxes faster, the curves cross, and the Mpemba effect takes place.

If we consider a one-parameter family of states, m evaluated for infinitesimally closed states is related to the derivative of ΔS_0 with respect to the parameter. The sign of the derivative governs whether the Mpemba effect occurs locally around a given state. The result is that the Mpemba effect occurs only in some regions of parameter space. To illustrate this point, we analyze two cases: varying η at fixed Δ, and varying Δ at fixed η. In the first case we always observe the Mpemba effect, while in the second case we only observe it using subsystems with $\ell > \eta$ and for sufficiently small conformal dimensions.

4.4.1. *Varying η at fixed Δ.* This is illustrated in Fig. 7. We always observe the Mpemba effect because any two curves cross. This can be understood from the fact that the initial value $\Delta S_0(\eta)$ is a decreasing function of η (see Fig. 8) and that the thermalization timescale t_* is an increasing function of η.

Downloaded from https://academic.oup.com/ptep/article/2025/6/063B05/8140051 by SISSA - Scuola Internazionale Superiore di Studi Avanzati user on 15 June 2026

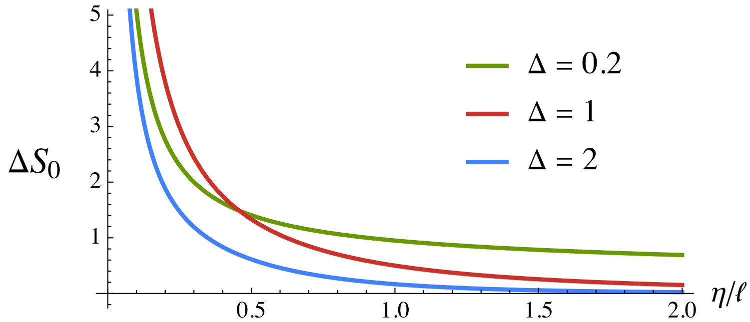

Fig. 8. The initial value $\Delta S_0(\eta) = \eta^{2\Delta} \Delta S^{(2)}_{\text{disk}}$ is a decreasing function of η for any fixed Δ. Since the thermalization timescale t_* is an increasing function of η, we always observe the Mpemba effect among states of different η and the same Δ, as illustrated in Fig. 7.

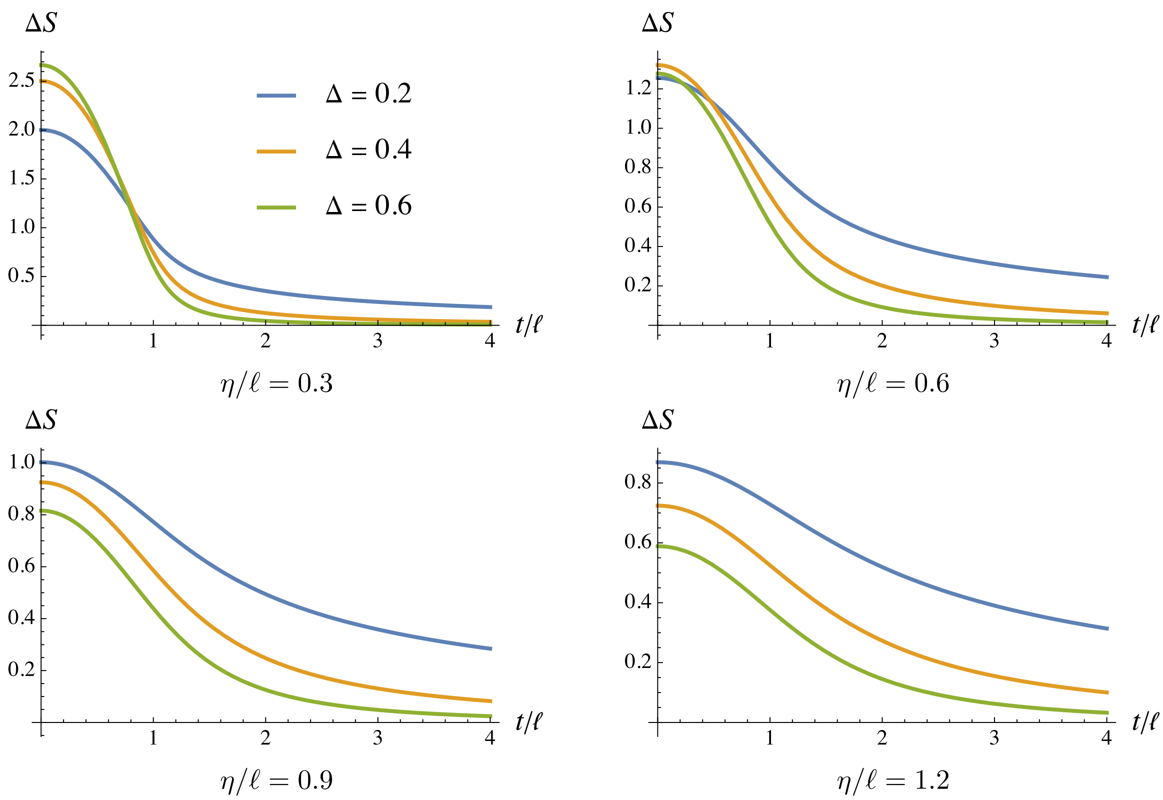

Fig. 9. Thermalization for different values of Δ and η. We observe different behaviors in different regions of parameter space. The Mpemba effect is only visible in the two upper plots.

4.4.2. *Varying Δ at fixed η.* As illustrated in Fig. 9, we observe two different behaviors depending on the values of the parameters. The two regimes originate from two different profiles of the initial-value curve $\Delta S_0(\Delta)$ plotted in Fig. 10. If dimension Δ is above a critical value Δ_* then the Mpemba effect does not take place. If $\Delta < \Delta_*$ then there is a Mpemba effect, but this is only visible in subsystems A with $\ell > \eta$. This is because at least one of the two conformal dimensions must be below the value Δ_* at which ΔS_0 has a maximum: the condition to observe the Mpemba effect is that $\Delta < \Delta'$ with $\Delta S_0(\Delta) < \Delta S_0(\Delta')$, which is possible only if $\Delta < \Delta_*$ and only in the region $\ell > \eta$.

Downloaded from https://academic.oup.com/ptep/article/2025/6/063B05/8140051 by SISSA - Scuola Internazionale Superiore di Studi Avanzati user on 15 June 2026

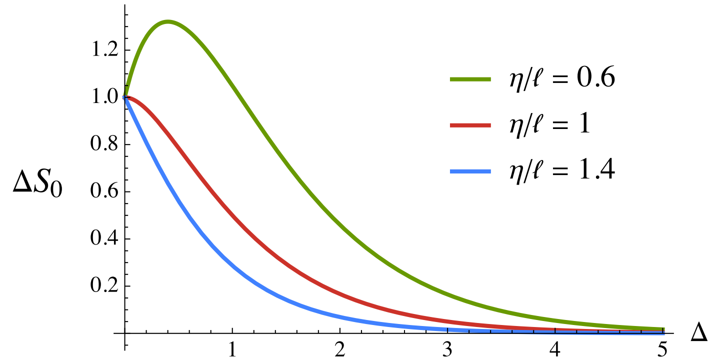

Fig. 10. The curve $\Delta S_0(\Delta) = \eta^{2\Delta} \Delta S^{(2)}_{\text{disk}}$ has two different shapes depending on the value of parameter η. For $\eta \geq \ell$, it is decreasing, while for $\eta < \ell$, it first increases and then decreases.

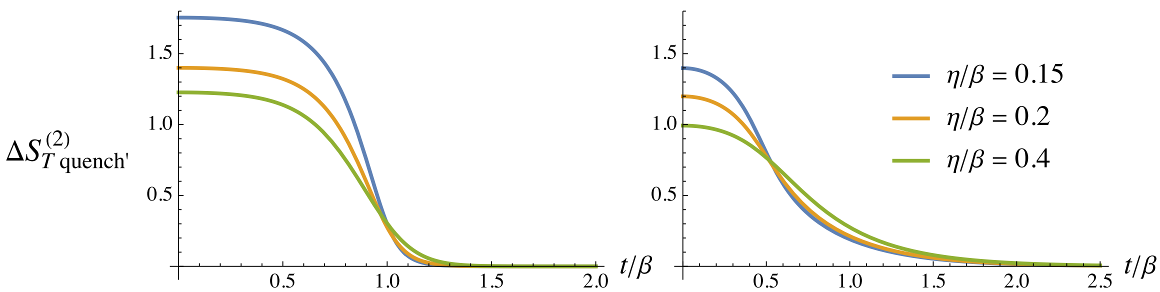

Fig. 11. Relaxation of entanglement asymmetry $\Delta S^{(2)}_{\text{T quench}'}(t) = \eta^{2\Delta} \Delta S^{(2)}_{\text{T quench}}(t)$ at finite temperature β^{-1} for different values of the parameters. Left: $\Delta = 1$ and $\ell/\beta = 1$. Right: $\Delta = 0.2$ and $\ell/\beta = \frac{1}{2}$.

4.4.3. *Finite temperature or volume.* Next, we can study the finite-temperature case given by $\Delta S^{(2)}_{\text{T quench}}(t)$ in Eq. (76). At late times the conformal factor behaves as $\Omega \sim 4\pi T \sinh(2\pi T \ell)\, e^{-2\pi T t}$, where $T = \beta^{-1}$ is the temperature, while $x \to 0$. This means that at nonvanishing temperature the late-time asymmetry decays exponentially:

$$\Delta S \sim \epsilon^2 \frac{\sqrt{\pi}\,\Gamma(\Delta+1)}{2\,\Gamma(\Delta+3/2)} [2\pi T \eta \sinh(2\pi T \ell)]^{2\Delta} e^{-4\pi \Delta T t} \quad \text{for } t \to \infty. \tag{85}$$

The natural thermalization timescale is

$$t_* = \frac{1}{\Delta T}. \tag{86}$$

The entanglement asymmetry is approximately constant for small times, and then it decays exponentially, as illustrated in Fig. 11. For what regards the Mpemba effect, there are four possible regimes depending on the shape of the curve $\Delta S_0(\Delta)$, distinguished by whether $\lim_{\Delta\to\infty} \Delta S_0$ vanishes or diverges, and by the sign of $\partial_\Delta \Delta S_0|_{\Delta=0}$. The four phases are as follows.

- The curve ΔS_0 is a monotonously decreasing function of Δ: we never see the Mpemba effect.
- The curve ΔS_0 first increases and then it decays with Δ: we observe the Mpemba effect for sufficiently small conformal dimensions.
- The curve ΔS_0 is monotonously increasing with Δ: we always observe the Mpemba effect.
- The curve ΔS_0 is first decreasing and then diverging with Δ: we see the Mpemba effect for sufficiently large conformal dimensions.

Downloaded from https://academic.oup.com/ptep/article/2025/6/063B05/8140051 by SISSA - Scuola Internazionale Superiore di Studi Avanzati user on 15 June 2026

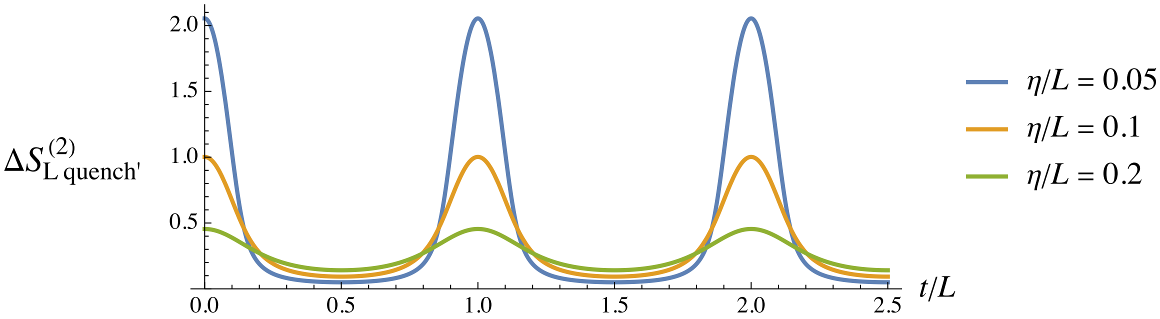

Fig. 12. Thermalization in finite volume described by $\Delta S^{(2)}_{\text{L quench}'}(t) = \eta^{2\Delta}\Delta S^{(2)}_{\text{L quench}}(t)$ for different values of η. We chose $\Delta = 1$ and subsystem size $\ell = L/8$. We observe a periodic behavior with period L.

Finally, let us briefly study the time evolution of entanglement asymmetry in finite volume. In Fig. 12 we plot the time dependence of $\Delta S^{(2)}_{\text{L quench}}(t)$ in Eq. (78) for different values of parameter η (that controls insertions along the central line) and a choice of Δ. We observe that the asymmetry is periodic with period L (the circumference of the sphere) and thus it never thermalizes. Although oscillations and partial revivals are expected in systems in finite volume (see, for instance, [45] for a discussion in two-dimensional rational CFTs), we do not expect exact periodicity in a generic CFT. We believe that this is an artifact of the perturbative expansion that will be corrected by higher-order terms.

5. Asymmetry in holography

The AdS/CFT correspondence [46–48] provides a nonperturbative definition of quantum gravity in AdS space in terms of a CFT that lives at the boundary, such that the bulk direction emerges from the strongly coupled many-body dynamics of the CFT. Quantum information theory has long been recognized to play a primary role in understanding the emergence of the bulk. The Ryu–Takayanagi formula [49] shows that complicated quantum-information quantities in the CFT can translate to simple geometric observables in AdS, which can sometimes be derived using a gravitational version of the replica trick [50–52]. Thus, it is natural to expect that entanglement asymmetry is also dual to a simple quantity in the bulk. In this section we provide some evidence for this, at least at leading order in parameter λ.

5.1. *Holographic setup*

A holographic CFT$_d$ on $\mathbb{R}^d$ is dual to a bulk gravitational theory in Euclidean AdS$_{d+1}$ with metric (in Poincaré coordinates)

$$ds^2 = \frac{dz^2 + dx_1^2 + \cdots + dx_d^2}{z^2}. \tag{87}$$

On the boundary we consider states obtained by turning on a source for a charged primary operator V in the Euclidean past:

$$|\psi\rangle = e^{i\int d^dx\lambda(x)V(x)}|0\rangle. \tag{88}$$

Such states are of particular interest in holography because they correspond to classical bulk states (see [32] and the references therein). When V is charged under a $U(1)$ symmetry, state $|\psi\rangle$ has nontrivial entanglement asymmetry.

Downloaded from https://academic.oup.com/ptep/article/2025/6/063B05/8140051 by SISSA - Scuola Internazionale Superiore di Studi Avanzati user on 15 June 2026

The charged primary V of conformal dimension Δ is dual to a complex scalar field ϕ in the bulk, and its source $\lambda(x)$ corresponds to a boundary condition

$$\lim_{z\to 0} z^{\Delta-d}\phi(z,x) = \lambda(x). \tag{89}$$

The matter theory in the bulk has Euclidean action:

$$S = \int dz\, d^d x \sqrt{g}\left(\frac{1}{4}F_{\mu\nu}F^{\mu\nu} + |D_\mu\phi|^2 + m^2|\phi|^2\right). \tag{90}$$

Here $D_\mu\phi = \nabla_\mu\phi - ieA_\mu\phi$ and the mass is related to the dimension of V via the formula $m^2 = \Delta(\Delta - d)$. The equations of motion are

$$(D_\mu D^\mu - m^2)\phi = 0, \qquad \nabla^\nu F_{\mu\nu} = j_\mu \quad \text{with} \quad j_\mu = -i(\phi^\dagger D_\mu\phi - \phi D_\mu\phi^\dagger), \tag{91}$$

where j_μ is the bulk current. The solution that satisfies the boundary condition (89) can be written as [48,53]

$$\phi(z,x) = \int d^d x' K_E(z,x\,|\,x')\lambda(x'), \tag{92}$$

where the bulk-to-boundary propagator is (for $\Delta > d/2$)

$$K_E(z,x\,|\,x') = C_\Delta\left(\frac{z}{z^2 + (x-x')^2}\right)^\Delta. \tag{93}$$

The value of C_Δ that reproduces Eq. (89) is $C_\Delta = \Gamma(\Delta)/[\pi^{d/2}\,\Gamma(\Delta - d/2)]$.[17] However, with that value, the resulting two-point function of the dual complex scalar operator V has coefficient $c = 2(2\Delta - d)\Gamma(\Delta)/[\pi^{d/2}\Gamma(\Delta - d/2)]$ (see the Appendix of [53]). In the field theory analysis we normalized operator V so that its two-point function has coefficient 1. In order to have the same normalization in holography, we should rescale field ϕ by $c^{-1/2}$. This is the same as rescaling K_E, namely, as taking

$$C_\Delta = \sqrt{\frac{\Gamma(\Delta)}{4\pi^{d/2}\Gamma(\Delta + 1 - d/2)}} \tag{94}$$

in Eq. (93). Note that the unitarity bound guarantees that $\Delta + 1 - d/2 > 0$.

We focus on states where the operator is inserted at a single point, i.e.

$$\lambda(x) = \lambda\delta^d(x - x_0), \tag{95}$$

and we take $\lambda \in \mathbb{R}$. We consider spherical regions A in the CFT, such that the modular Hamiltonian is local and related to the boost generators of half-space by a conformal transformation [54]. As explained in Section 4, the reduced density matrix of A can be obtained by using a different time slicing of $\mathbb{R}^d$. This corresponds to writing the metric of $\mathbb{R}^d$ as a conformal transformation of $S^1 \times \mathbb{H}^{d-1}$, namely, as

$$ds^2 = \Omega^{-2}[d\tau^2 + du^2 + \sinh^2(u)\, d\Omega^2_{d-2}], \tag{96}$$

as we already did in Section 4.1. The conformal factor (57) in these coordinates (for $\ell = 1$) is

$$\Omega = \cosh(u) + \cos(\tau). \tag{97}$$

The spherical region A is mapped to the whole hyperbolic plane $\mathbb{H}^{d-1}$ at $\tau = 0$. In the bulk this slicing means writing the AdS metric using coordinates adapted to the Rindler wedge:

$$ds^2 = (\rho^2 - 1)\, d\tau^2 + \frac{d\rho^2}{\rho^2 - 1} + \rho^2[du^2 + \sinh^2(u)\, d\Omega^2_{d-2}] \tag{98}$$

[17] For the case $\Delta = d/2$ in which the mass is at the Breitenlohner–Freedman bound, the asymptotic behavior and the normalizations are different [53].

Downloaded from https://academic.oup.com/ptep/article/2025/6/063B05/8140051 by SISSA - Scuola Internazionale Superiore di Studi Avanzati user on 15 June 2026

with $\rho > 1$. In these coordinates the bulk-to-boundary propagator (93) in the embedding formalism reads

$$K_E(\rho, \tau, Y \mid \tau', Y') = \frac{C_\Delta}{[-2\rho Y \cdot Y' - 2\sqrt{\rho^2 - 1}\cos(\tau - \tau')]^\Delta}. \tag{99}$$

Here $Y = \left(Y_0, Y_{a=1,\dots,d-1}\right)$ are coordinates on the hyperboloid $\mathbb{H}^{d-1}$; they solve the constraint $Y \cdot Y \equiv -Y_0^2 + \sum_a Y_a^2 = -1$ and are parametrized as $Y = [\cosh(u), \sinh(u)\theta_a]$ with $\sum_a \theta_a^2 = 1$ so that $\theta_a \in S^{d-2}$ (see Appendix D and Appendix A of [32] for more details). The Rindler horizon is at $\rho = 1$ and the asymptotic boundary is at $\rho = \infty$. The prescription of [32], as we review below, requires us to construct a real-time solution for the bulk fields. In particular, the bulk solution is constructed by analytically continuing propagator (99) to $\tau \to it$. It is then useful at this stage to perform the analytic continuation $\tau = it$ to the Lorentzian signature in Eq. (98) as well, where t is the Lorentzian Rindler time. In these coordinates the bulk modular flow in the Rindler wedge is represented by the manifest Killing symmetry

$$\xi = 2\pi\, \partial_t. \tag{100}$$

The prescription of [32] then, given a spherical region in the CFT$_d$ on $S^1 \times \mathbb{H}^{d-1}$ as before and a one-parameter family of excited states $\rho_A = \sigma_A[1 + i\int d^d x \lambda(x) V(x) + \text{H.c.} + \cdots]$, requires us to construct bulk solutions consistent with the operator insertions on the boundary. In hyperbolic coordinates, Eq. (92) reads

$$\phi(\rho, t, Y) = \int d\tau'\, dY'\, K_E(\rho, it, Y \mid \tau', Y')\lambda(\tau', Y') \tag{101}$$

with K_E as defined in Eq. (99) but analytically continued to $\tau \to it$.

Let us construct these solutions explicitly in Lorentzian AdS$_{d+1}$. The boundary CFT has delta-function sources corresponding to the Euclidean insertion of two conjugate operators V at $\tau' = -(\pi - \tau_0)$ and $V^\dagger$ at $\tau' = (\pi - \tau_0)$. Without loss of generality we take $u' = 0$. The solution takes the form $\phi(\rho, t, u) = \lambda K_E(\rho, it, u \mid \tau_0 - \pi, 0)$ and similarly for $\phi^\dagger$:

$$\begin{aligned} \phi &= \frac{\lambda C_\Delta}{[2\rho\cosh(u) + 2\sqrt{\rho^2 - 1}\cos(it - \tau_0)]^\Delta}, \\ \phi^\dagger &= \frac{\lambda C_\Delta}{[2\rho\cosh(u) + 2\sqrt{\rho^2 - 1}\cos(it + \tau_0)]^\Delta}. \end{aligned} \tag{102}$$

Note that inserting the boundary operators at specular points $\tau' = \mp(\pi - \tau_0)$ automatically ensures that the bulk solutions are complex conjugate to each other.

5.2. *Asymmetry as canonical energy*

We saw that, at leading order, entanglement asymmetry is equal to perturbative relative entropy. The latter was shown in [32,36] to be holographically dual to canonical energy, first defined by Hollands and Wald [55] and then generalized in [56,57]. This defines a metric on the space of perturbations, known as the "quantum Fisher" or Bogoliubov–Kubo–Mori metric. We therefore conclude that the leading-order entanglement asymmetry is given by the canonical energy, where we are interested in the particular case of scalar primary operator insertions on the boundary, and corresponding dual bulk scalar fields. The canonical energy is defined as a particular symplectic flux of on-shell fields, evaluated on a codimension-one surface in the entanglement wedge that is bounded by the Ryu–Takayanagi surface $\widetilde{A}$ on one side and by the boundary subsystem A on the other side. Since the symplectic flux is conserved, we are free to

Downloaded from https://academic.oup.com/ptep/article/2025/6/063B05/8140051 by SISSA - Scuola Internazionale Superiore di Studi Avanzati user on 15 June 2026

choose any such surface and we choose the $t = 0$ spatial slice of the entanglement wedge.[18] We denote such a surface as Σ, whose boundary is $\partial\Sigma = A \cup \widetilde{A}$. The bulk formula for the entanglement asymmetry is

$$\Delta S = \int_\Sigma \star\,\boldsymbol{\omega}(\phi, \mathcal{L}_\xi\phi) + O(\lambda^4), \tag{103}$$

where ϕ is taken of order λ. Here ξ is the vector field of bulk modular flow, which in Rindler coordinates is Eq. (100), while $\mathcal{L}_\xi$ is a Lie derivative. We stress that A should be a half-space, a spherical region, or a conformal transformation thereof, in order for the modular flow ξ to be geometric and Eq. (103) to be applicable. The symplectic current $\boldsymbol{\omega}$ is a one-form, quadratic in the on-shell bulk fields (102). We also expect corrections suppressed by G_N and e obtained by taking into account the gravitational and gauge fields.

The symplectic current can be derived by writing the variation of the bulk Lagrangian under a field variation [58]:

$$\delta\mathscr{L} = E_\phi\delta\phi + \nabla^\mu\Theta_\mu[\delta\phi] \tag{104}$$

with E_ϕ the equations of motion. The quantity Θ_μ that produces a total derivative is called the presymplectic current. The symplectic current is then defined as [58]

$$\boldsymbol{\omega}_\mu(\delta_1\phi, \delta_2\phi) = \delta_1\Theta_\mu[\delta_2\phi] - \delta_2\Theta_\mu[\delta_1\phi]. \tag{105}$$

For the bulk action (90), and working in the approximation that only the complex scalar field is turned on at leading order, we find that

$$\begin{aligned} \Theta_\mu[\delta\phi] &= (D_\mu\phi)\delta\phi^\dagger + (D_\mu\phi^\dagger)\delta\phi, \\ \boldsymbol{\omega}_\mu(\phi_1, \phi_2) &= (D_\mu\phi_1)\phi_2^\dagger + (D_\mu\phi_1^\dagger)\phi_2 - (D_\mu\phi_2)\phi_1^\dagger - (D_\mu\phi_2^\dagger)\phi_1. \end{aligned} \tag{106}$$

The surface Σ is at $t = 0$. This surface has normal vector $n = (\rho^2 - 1)^{-1/2}\,\partial_t$ and induced spatial metric

$$ds^2\Big|_{t=0} = \frac{d\rho^2}{\rho^2 - 1} + \rho^2[du^2 + \sinh^2(u)\,d\Omega_{d-2}^2] \equiv h_{ab}\,dx^a dx^b. \tag{107}$$

The holographic result for the entanglement asymmetry is then

$$\Delta S = \int_1^\infty d\rho \int_0^\infty du \int_{S^{d-2}} d\Omega_{d-2}\,\sqrt{h}\,n^\mu\boldsymbol{\omega}_\mu(\phi, \mathcal{L}_\xi\phi) + O(\lambda^4). \tag{108}$$

Inserting the solutions (102), the integrand takes the explicit form[19]

$$\begin{aligned} &\int d\Omega_{d-2}\,\sqrt{h}\,n^\mu\boldsymbol{\omega}_\mu(\phi, \mathcal{L}_\xi\phi)\Big|_{t=0} \\ &= \lambda^2\frac{C_\Delta^2\,\mathrm{Vol}_{S^{d-2}}\pi\,\Delta\rho^{d-1}\sinh^{d-2}(u)[1 + 2\Delta\sin^2(\tau_0) + \rho(\rho^2-1)^{-1/2}\cos(\tau_0)\cosh(u)]}{4^{\Delta-1}[\rho\cosh(u) + \sqrt{\rho^2-1}\cos(\tau_0)]^{2(\Delta+1)}}. \end{aligned} \tag{109}$$

Note that the integral in ρ converges if Δ is larger than the unitarity bound. Although the integral is hard to perform analytically, it is easy to evaluate numerically and we verified that it precisely reproduces the CFT answer:

$$\int_1^\infty d\rho \int_0^\infty du \int d\Omega_{d-2}\,\sqrt{h}\,n^\mu\boldsymbol{\omega}_\mu(\phi, \mathcal{L}_\xi\phi) = \lambda^2\Delta S^{(2)}_{\text{hyper}}, \tag{110}$$

as given explicitly by Eq. (50).

[18] The choice made in [32] is instead that Σ is the horizon of the entanglement wedge.

[19] Recall that $\mathrm{Vol}_{S^{d-2}} = 2\pi^{(d-1)/2}/\Gamma[(d-1)/2]$.

Downloaded from https://academic.oup.com/ptep/article/2025/6/063B05/8140051 by SISSA - Scuola Internazionale Superiore di Studi Avanzati user on 15 June 2026

5.3. *Relation to the bulk charge*

In holography a bulk gauge field A_μ is dual to a boundary current operator. However, there also exists a *bulk* current that, for the action in Eq. (90), takes the form

$$j_\mu = -i(\phi^\dagger D_\mu \phi - \phi D_\mu \phi^\dagger). \tag{111}$$

This is written in Lorentzian signature where Hermitian conjugation acts in the standard way. Note that the bulk current is a rather mysterious quantity from the point of view of the boundary CFT. A natural observable is the bulk charge of the Rindler wedge:

$$Q_{\text{bulk}} = \int_\Sigma \star j. \tag{112}$$

In AdS_{d+1} it takes the explicit form $Q_{\text{bulk}} = \int_1^\infty d\rho \int_0^\infty du \int d\Omega_{d-2} \sqrt{h}\, n^\mu j_\mu$ and the integrand reads

$$\int d\Omega_{d-2}\sqrt{h}\, n^\mu j_\mu \bigg|_{t=0} = -\lambda^2 \frac{C_\Delta^2 \text{Vol}_{S^{d-2}} 2\Delta \rho^{d-1} \sinh^{d-2}(u) \sin(\tau_0)}{4^\Delta \sqrt{\rho^2-1}[\rho\cosh(u) + \sqrt{\rho^2-1}\cos(\tau_0)]^{2\Delta+1}}. \tag{113}$$

Using the equation of motion $d \star F = \star j$, we can write the integral as

$$Q_{\text{bulk}} = \int_A \star F - \int_{\widetilde{A}} \star F, \tag{114}$$

where we have used the fact that the boundary of the surface Σ is the union of the boundary subsystem A and the Ryu–Takayanagi surface $\widetilde{A}$. The first term simply computes the expectation value of the $U(1)$ charge Q in the CFT, i.e.

$$\int_A \star F = \text{Tr}(\rho Q), \tag{115}$$

while the second term is the electric flux through the Ryu–Takayanagi surface.

Now, one might expect a relation between bulk charge and entanglement asymmetry. Indeed, we observe that, in our setup, the following simple relation holds:

$$\lambda^2 \Delta S^{(2)} = -2\pi \partial_{\tau_0} Q_{\text{bulk}}. \tag{116}$$

This follows from the fact that the integrand satisfies (for any t)

$$\boldsymbol{\omega}_\mu(\phi, \mathcal{L}_\xi \phi) = -2\pi \partial_{\tau_0} j_\mu. \tag{117}$$

This can be checked explicitly from the formulas given above. It can also be argued from the fact that ∂_{τ_0} acts as $i\partial_t$ on ϕ, while it acts as $-i\partial_t$ on $\phi^\dagger$ in Eq. (102), due to the general form of the bulk-to-boundary propagator. Indeed, a simple calculation shows that

$$\boldsymbol{\omega}_\mu(\phi, \mathcal{L}_\xi \phi) = [(\partial_\mu \phi)(2\pi \partial_t \phi^\dagger) - (2\pi \partial_\mu \partial_t \phi)\phi^\dagger] + \text{H.c.} = -2\pi \partial_{\tau_0} j_\mu. \tag{118}$$

This equation is reminiscent of the general analysis carried out in the context of black hole mechanics and Noether charges associated with the symmetries on the black hole horizon [59,60]. It would be interesting to investigate this point more systematically.

Note that τ_0 parametrizes a one-parameter family of solutions as in Eq. (102), with delta-function sources. One could generalize this setting to a one-parameter family of smeared complex sources labeled by a parameter α:

$$\lambda_\alpha(\tau, Y) = \lambda_0(\tau - \alpha, Y), \qquad \lambda_\alpha^*(\tau, Y) = \lambda_0^*(\tau + \alpha, Y), \tag{119}$$

with λ_0 and λ_0^* some reference sources. The effect of α is to shift the boundary conditions along the modular flow. The bulk solutions are then labeled by α as

$$\phi_\alpha(\rho, t, Y) = \int d\tau' \, dY' K_E(\rho, it, Y \mid \tau', Y') \lambda_\alpha(\tau', Y'). \tag{120}$$

Downloaded from https://academic.oup.com/ptep/article/2025/6/063B05/8140051 by SISSA - Scuola Internazionale Superiore di Studi Avanzati user on 15 June 2026

Since $\partial_\tau \lambda_\alpha = -\partial_\alpha \lambda_\alpha$ and K_E has translational invariance, one can trade the derivatives with respect to t, τ', and α using integration by parts:

$$\mathcal{L}_\xi \phi_\alpha = -2\pi i \partial_\alpha \phi_\alpha, \qquad \mathcal{L}_\xi \phi^\dagger_\alpha = 2\pi i \partial_\alpha \phi^\dagger_\alpha. \tag{121}$$

With this, the holographic answer can be written as

$$\Delta S^{(2)} = -2\pi\, \partial_\alpha \int_\Sigma \star\, j_\alpha, \tag{122}$$

where both sides are of order λ^2. In other words, the holographic formula (116) for the quadratic entanglement asymmetry can be interpreted as the derivative of the bulk charge of the entanglement wedge, with respect to a modular flow of the sources that create the state. It would be interesting to better understand the physical meaning of this observation.

Funding

Open Access funding: SCOAP^3.

Acknowledgments

We are grateful to Filiberto Ares, Pasquale Calabrese, Laurent Freidel, Giovanni Galati, Max Metlitski, and Sridip Pal for helpful discussions. We acknowledge support from ERC-COG grant NP-QFT No. 864583 "Non-perturbative dynamics of quantum fields: from new deconfined phases of matter to quantum black holes," from MUR-FARE grant EmGrav No. R20E8NR3HX "The Emergence of Quantum Gravity from Strong Coupling Dynamics," from MUR-PRIN2022 grant No. 2022NY2MXY, and from the INFN "Iniziativa Specifica ST&FI."

Appendix A. Renyi asymmetries in 2D CFTs

We compute the Renyi asymmetries in Eq. (28) for a few semi-integer values of Δ. In particular, we have to evaluate the sums

$$P_n = \sum_{j\neq k}^{n} \frac{1}{|2\sin[\pi(j-k+\tau_0/\pi)/n]|^{2\Delta}}\,. \tag{A1}$$

We use the Mellin transform (29) of $1/\sin(\pi x)$.

Case $\Delta = 1/2$. Taking into account the fact that $\tau_0 \in (0, \pi)$ and therefore, for $j > k$, the argument of the sine is between 0 and π, while for $j < k$, it is between $-\pi$ and 0, we have

$$\begin{aligned}\Delta S_n^{(2)} &= \frac{n^{-1}}{n-1}\frac{1}{r}\int \frac{ds}{2\pi(1+e^s)}\left[\sum_{j>k}^{n} e^{s(j-k+\tau_0/\pi)/n} + \sum_{j<k}^{n} e^{s(j-k+\tau_0/\pi+n)/n}\right] \\ &= \frac{n^{-1}}{n-1}\frac{1}{r}\int ds \frac{n(e^{s/n}-e^s)}{2\pi(1+e^s)(1-e^{s/n})} e^{s\tau_0/n\pi}.\end{aligned} \tag{A2}$$

We can now take the limit $\Delta S^{(2)} = \lim_{n\to 1} \Delta S_n^{(2)}$, yielding

$$\Delta S^{(2)} = \frac{1}{r}\int \frac{ds\, s e^{s\tau_0/\pi}}{4\pi \sinh(s)} = \frac{1}{r}\frac{\pi}{8\cos^2(\tau_0/2)}. \tag{A3}$$

Downloaded from https://academic.oup.com/ptep/article/2025/6/063B05/8140051 by SISSA - Scuola Internazionale Superiore di Studi Avanzati user on 15 June 2026

Case $\Delta = 1$. We proceed as before; however, this time there are two integrations:

$$P_n = \frac{1}{4\pi^2}\int \frac{ds_1\, ds_2}{(1+e^{s_1})(1+e^{s_2})}\left[\sum_{j>k}^{n} e^{(s_1+s_2)(j-k+\tau_0/\pi)/n} + \sum_{j<k}^{n} e^{(s_1+s_2)(j-k+\tau_0/\pi+n)/n}\right]$$

$$= \frac{1}{4\pi^2}\int ds_1\, ds_2 \frac{n(e^{(s_1+s_2)/n} - e^{s_1+s_2})}{(1+e^{s_1})(1+e^{s_2})(1-e^{(s_1+s_2)/n})} e^{(s_1+s_2)\tau_0/n\pi}. \tag{A4}$$

The integral can be computed analytically. First we change variables, setting $s_2 = s - s_1$ and perform the integral in s_1, obtaining

$$P_n = \int ds\, \frac{ns}{8\pi^2} e^{s\tau_0/n\pi}\left(\frac{1}{\tanh(s/2n)} - \frac{1}{\tanh(s/2)}\right). \tag{A5}$$

Then we shift the integration contour from $\mathbb{R}$ to $\mathbb{R} + \pi i$ by redefining $s \to s + \pi i$, as this does not cross any pole of the integrand. We perform indefinite integration in τ_0 to simplify the expression, and finally integrate in s. We obtain

$$P_n = \partial_{\tau_0}\left[\frac{n^2}{4}\left(\frac{1}{\tan(\tau_0/n)} - \frac{n}{\tan(\tau_0)} - i(n-1)\right)\right] = \frac{n^3}{4\sin^2(\tau_0)} - \frac{n}{4\sin^2(\tau_0/n)}. \tag{A6}$$

This yields the Renyi asymmetry

$$\Delta S_n^{(2)} = \frac{1}{4r^2}\,\frac{n}{n-1}\left(\frac{1}{\sin^2(\tau_0)} - \frac{1}{n^2\sin^2(\tau_0/n)}\right) \tag{A7}$$

and the entanglement asymmetry

$$\Delta S^{(2)} = \frac{1}{2r^2\sin^2(\tau_0)}\left(1 - \frac{\tau_0}{\tan(\tau_0)}\right). \tag{A8}$$

Case $\Delta = 3/2$. This time the Renyi asymmetry is given by three integrations:

$$\Delta S_n^{(2)} = \frac{n^{-2}}{n-1}\frac{1}{r^3}\int \frac{ds_1\, ds_2\, ds_3}{8\pi^3(1+e^{s_1})(1+e^{s_2})(1+e^{s_3})}\frac{e^{s/n} - e^{s}}{1-e^{s/n}} e^{s\tau_0/n\pi} \tag{A9}$$

with $s = s_1 + s_2 + s_3$. Taking the limit $n \to 1$ we obtain the entanglement asymmetry

$$\Delta S^{(2)} = \frac{1}{8\pi^3 r^3}\int \frac{ds_1\, ds_2\, ds_3}{(1+e^{s_1})(1+e^{s_2})(1+e^{s_3})}\frac{s e^{s\tau_0/\pi}}{1-e^{-s}}. \tag{A10}$$

It is convenient to change variables to s_1, s_2, s. The integral in s_1 can be easily performed:

$$\Delta S^{(2)} = \frac{1}{8\pi^3 r^3}\int ds_2\, ds\, \frac{s(s-s_2)e^{s\tau_0/\pi}}{(1+e^{-s_2})(e^{s} - e^{s_2})(1-e^{-s})}. \tag{A11}$$

Then we shift the integration contour $s \to s + \pi i$. The integral in s_2 gives

$$\Delta S^{(2)} = \frac{e^{i\tau_0}}{8\pi^3 r^3}\int ds \frac{s(s+\pi i)(s+2\pi i)e^{s\tau_0/\pi}}{2(1+e^{-s})(1-e^{s})}. \tag{A12}$$

The final integral gives the entanglement asymmetry

$$\Delta S^{(2)} = \frac{3\pi}{128 r^3\cos^4(\tau_0/2)}. \tag{A13}$$

Case $\Delta = 2$. The Renyi asymmetry is given by four integrations. After taking the limit $n \to 1$ and changing variables to $s = s_1 + s_2 + s_3 + s_4$, we obtain the expression

$$\Delta S^{(2)} = \frac{1}{(2\pi r)^4}\int \frac{ds\, ds_1\, ds_2\, ds_3\; s e^{s_1+s_2+s_3} e^{s\tau_0/\pi}}{(1+e^{s_1})(1+e^{s_2})(1+e^{s_3})(e^{s_1+s_2+s_3} + e^{s})(1-e^{-s})}. \tag{A14}$$

We perform the integral in s_1, and then shift the integration contour $s \to s + \pi i$:

$$\Delta S^{(2)} = \frac{e^{i\tau_0}}{(2\pi r)^4}\int ds\, ds_2\, ds_3 \frac{(s+\pi i)(s_2+s_3-s-\pi i)e^{s\tau_0/\pi}}{(1+e^{-s_2})(1+e^{-s_3})(e^{s_2+s_3} + e^{s})(1+e^{-s})}. \tag{A15}$$

Downloaded from https://academic.oup.com/ptep/article/2025/6/063B05/8140051 by SISSA - Scuola Internazionale Superiore di Studi Avanzati user on 15 June 2026

We perform the integral in s_2, and then shift the integration contour back as $s \to s - \pi i$:

$$\Delta S^{(2)} = \frac{1}{(2\pi r)^4} \int ds\, ds_3 \frac{s(s - s_3 - \pi i)(s - s_3 + \pi i)e^{s\tau_0/\pi}}{2(1 + e^{-s_3})(e^{s_3} + e^s)(1 - e^{-s})}. \tag{A16}$$

We perform the integral in s_3:

$$\Delta S^{(2)} = \frac{1}{(2\pi r)^4} \int ds\, \frac{s^2(s^2 + 4\pi^2)e^{s\tau_0/\pi}}{6(e^s - 1)(1 - e^{-s})}. \tag{A17}$$

The final integration gives the entanglement asymmetry

$$\Delta S^{(2)} = \frac{1}{4r^4 \sin^4(\tau_0)} \left(1 - \frac{1}{3}\sin^2(\tau_0) - \frac{\tau_0}{\tan(\tau_0)}\right). \tag{A18}$$

Appendix B. Computation from relative entropy

Let us give some details on the evaluation of integral (42),

$$I_\Delta = -\int_{\mathbb{R}} ds\, \frac{1}{4\sinh^2(s/2 - i\varepsilon)[-4\sinh^2(s/2 - i\tau_0)]^\Delta}, \tag{B1}$$

in terms of the function $I_\Delta(x)$ in Eq. (43) with $x = \tan(\tau_0/2)$.

First note that, calling $f(s)$ the integrand in Eq. (B1), it satisfies $f(-s^*) = f(s)^*$. Since the operation $s \to -s^*$ maps the part of the contour with $s > 0$ to the part with $s < 0$, this implies that the integral can be written as

$$I_\Delta = \int_0^\infty \mathbb{R}\mathrm{e}[f(s)], \tag{B2}$$

showing that the integral is always real. The integrand has poles at $s = 2i\varepsilon + 2\pi ik$ and $s = 2i\tau_0 + 2\pi ik$ for any $k \in \mathbb{Z}$. We thus shift the contour as $s \to s + 2i\tau_0 - \pi i$. For $0 < \tau_0 < \pi/2$, the contour is moved downward and it does not cross any pole of $f(s)$. On the contrary, for $\pi/2 < \tau_0 < \pi$, the contour is moved upward and it crosses the pole at $s = 2i\varepsilon$ where we pick up a residue. We thus obtain the expression

$$I_\Delta = J_\Delta - \delta_{\pi/2<\tau_0<\pi} \frac{2\pi\Delta}{4^\Delta \sin^{2\Delta}(\tau_0)\tan(\tau_0)}, \tag{B3}$$

where

$$\begin{aligned} J_\Delta &= \int_0^\infty \mathbb{R}\mathrm{e}\left[\frac{2^{-2\Delta-1}\, ds}{\cosh^2(s/2 + i\tau_0)\cosh^{2\Delta}(s/2)}\right] \\ &= \int_0^\infty \frac{[1 + \cos(2\tau_0)\cosh(s)]\, ds}{2^\Delta[\cos(2\tau_0) + \cosh(s)]^2[1 + \cosh(s)]^\Delta}. \end{aligned} \tag{B4}$$

To compute the integral, we perform the change of variable $t = \tanh^2(s/2)$ to obtain

$$J_\Delta = \int_0^1 dt \frac{(1 + X)(1 - tX)(1 - t)^\Delta}{2^{2\Delta+1}\sqrt{t}(1 + tX)^2}, \tag{B5}$$

where we have defined the parameter $X = \tan^2(\tau_0)$. This can be integrated as a hypergeometric function

$$J_\Delta = \frac{\sqrt{\pi}\,\Gamma(\Delta + 1)}{4^\Delta \Gamma(\Delta + 1/2)} \left(1 - \frac{\Delta}{\Delta + 1/2}\, {}_2F_1\left[\frac{1}{2}, 1, \Delta + \frac{3}{2}; -X\right]\right). \tag{B6}$$

The hypergeometric function has a branch cut from 1 to infinity, conventionally taken along the positive real axis. When $0 < \tau_0 < \pi/2$, the argument $-X$ of the hypergeometric function goes from 0 to infinity along the negative real axis. For $\tau_0 = \pi/2$, the argument reaches the branch point at infinity and it moves to the second sheet. When $\pi/2 < \tau_0 < \pi$, the argument goes from

Downloaded from https://academic.oup.com/ptep/article/2025/6/063B05/8140051 by SISSA - Scuola Internazionale Superiore di Studi Avanzati user on 15 June 2026

infinity to zero on the second sheet along the negative real axis. The fact that the argument is on the second sheet is implemented by the second term in Eq. (B3).

In order to obtain an equivalent expression that does not require moving between different sheets, it is useful to use a different parameter $x = \tan(\tau_0/2)$, related to X by

$$X = \frac{4x^2}{(x^2-1)^2}. \tag{B7}$$

Then one can use hypergeometric transformation identities (see, e.g. [61]) to rewrite the answer in terms of x, obtaining Eq. (43). A simple way to implement the transformation is to use the fact that the hypergeometric function $y(z) = {}_2F_1(a, b, c; z)$ satisfies a second-order differential equation:

$$z(1-z)y''(z) + [c-(a+b+1)z]y'(z) - ab\, y(z) = 0. \tag{B8}$$

This implies that the function $I_\Delta \equiv F(X)$ satisfies the differential equation

$$2X(X+1)F''(X) + (2\Delta + 5X + 3)F'(X) + F(X) = \frac{\sqrt{\pi}\,\Gamma(\Delta+1)}{4^\Delta\Gamma(\Delta+1/2)}. \tag{B9}$$

We then use the change of variable (B7) to write a differential equation for the function $I_\Delta \equiv f(x)$ in terms of parameter x:

$$\frac{(x^2-1)^2}{8}f''(x) - \frac{(x^2-1)[1+3x^2+(x^2-1)^2\Delta]}{4x(x^2+1)}f'(x) + f(x) = \frac{\sqrt{\pi}\,\Gamma(\Delta+1)}{4^\Delta\Gamma(\Delta+1/2)}. \tag{B10}$$

Solving this equation again gives the expression in Eq. (43).

Appendix C. Asymmetry from twist operators

As in [34], the Renyi asymmetries can be computed by making use of replicated theories, as opposed to replicated geometries. Given a theory $\mathcal{S}$, we consider a theory $\mathcal{S}^{(n)}$ made of n decoupled copies of $\mathcal{S}$. Since $\mathcal{S}^{(n)}$ has a permutation symmetry that exchanges the copies, it also has a codimension-two twist operator $\mathcal{T}_n$ such that, when we circle around it, we go from one copy to the next, cyclically. More precisely, $\mathcal{T}_n$ is the (nontopological) boundary of a codimension-one topological symmetry defect such that the fields on the two sides are glued with a cyclic permutation. If theory $\mathcal{S}$ has a $U(1)$ symmetry, the previous symmetry defect can be combined with other symmetry defects that implement independent $U(1)$ actions on each copy of $\mathcal{S}$ in $\mathcal{S}^{(n)}$. This generates a dressed twist operator $\mathcal{T}_{n,\gamma}$ that permutes the copies and besides acts with $e^{i\gamma_j Q_A}$ on the jth copy. The twist operators relevant for the computation of Renyi asymmetries have $\sum_j \gamma_j = 0 \bmod 2\pi$. Similarly to Eq. (17), the Renyi asymmetry is then given by a ratio of correlation functions, one with the insertion of the dressed twist fields, and one with the standard twist fields:

$$\Delta S_n = \frac{1}{1-n}\log\frac{[1/(2\pi)^{n-1}]\int d\vec{\gamma}\ \langle \mathcal{T}_{n,\gamma}[\partial A]\cdots\rangle}{\langle \mathcal{T}_n[\partial A]\cdots\rangle}. \tag{C1}$$

The twist fields are placed along the boundaries of the cut A. The dots stand for possible operator insertions used to construct the state.

In two dimensions the symmetry defects are lines and the twist operators are pointlike; therefore, Eq. (C1) boils down to the computation of certain correlation functions. In this appendix we use Eq. (C1) to compute the Renyi asymmetry of a 2D free Dirac fermion Ψ with respect to its vectorlike $U(1)$ symmetry, in coherent states generated by the primary[20] $V = \psi_L\psi_R$

[20] It can be written as $V = \Psi^\mathsf{T} C\Psi$, where C is the charge conjugation matrix.

Downloaded from https://academic.oup.com/ptep/article/2025/6/063B05/8140051 by SISSA - Scuola Internazionale Superiore di Studi Avanzati user on 15 June 2026

with $\Delta = 1$ for an interval $A = [-\ell, \ell]$. This computation will reproduce Eq. (60) for $\Delta = 1$, as well as a conformal transformation of Eq. (30).

The theory $\mathcal{S}^{(n)}$ is given by n copies Ψ_k $(k = 1, \dots, n)$ of the 2D free Dirac fermion. The twist operator $\mathcal{T}_{n,\gamma}(u)$ implements the boundary conditions[21]

$$\begin{aligned} \Psi_k(u + e^{2\pi i} w) &= e^{i\gamma_k} \Psi_{k+1}(u + w) \quad \text{for } k = 1, \dots, n-1, \\ \Psi_n(u + e^{2\pi i} w) &= (-1)^{n+1} e^{-i(\gamma_1 + \dots + \gamma_{n-1})} \Psi_1(u + w), \end{aligned} \tag{C2}$$

around u. The twist operator $\mathcal{T}^\dagger_{n,\gamma}$ implements the opposite boundary conditions. Writing $\gamma_k = \alpha_{k+1} - \alpha_k$, the boundary conditions are diagonalized by the fields

$$\tilde{\Psi}_l = \frac{1}{\sqrt{n}} \sum_{k=1}^{n} \exp\left(-2\pi i \frac{2l - n - 1}{2n} k + i\alpha_k \right) \Psi_k \tag{C3}$$

in the sense that

$$\tilde{\Psi}_l(u + e^{2\pi i} w) = e^{2\pi i m_l} \tilde{\Psi}_l(u + w) \quad \text{with} \quad m_l = \frac{2l - n - 1}{2n}. \tag{C4}$$

Note that in the diagonalizing basis the twists do not depend on the γ_k. We decompose the Dirac fermion $\Psi = \binom{\psi_L}{\psi_R}$ into left- and right-moving parts, and the two fields ψ_L and ψ_R have the same charge under $U(1)$. Then the scalar primary we use to construct the excited coherent states is $V = \psi_L \psi_R$.

In order to construct the twist operators, we use bosonization. For each copy $\tilde{\Psi}_l$, we introduce a compact scalar[22] $\varphi \cong \varphi + 2\pi$ and decompose it into left- and right-moving parts: $\varphi = \varphi_L + \varphi_R$ and $\tilde{\varphi} = \varphi_L - \varphi_R$. An operator $\mathcal{O} = e^{i\epsilon_L \varphi_L} e^{i\epsilon_R \varphi_R}$ has dimensions $(h, \bar{h}) = \left(\epsilon_L^2/2, \epsilon_R^2/2\right)$. It follows that the fermions are

$$\tilde{\psi}_L = e^{i\varphi_L}, \qquad \tilde{\psi}_L^\dagger = e^{-i\varphi_L}, \qquad \tilde{\psi}_R = e^{i\varphi_R}, \qquad \tilde{\psi}_R^\dagger = e^{-i\varphi_R}. \tag{C5}$$

The current that implements the shift symmetry $\varphi \to \varphi + \text{const}$ is $J_\mu = \partial_\mu \varphi / 2\pi$ and the charge operator is $Q = \int \star J = (1/2\pi) \int d\tilde{\varphi}$. The twist operator lives at the end of a symmetry defect. Thus, the operator that implements a twist by $e^{2\pi i \epsilon}$ along the positive real axis, which lives at the left end of the line $e^{2\pi i \epsilon Q}$, is $e^{i\epsilon\tilde{\varphi}} = e^{i\epsilon\varphi_L} e^{-i\epsilon\varphi_R}$ with dimensions $(h, \bar{h}) = (\epsilon^2/2, \epsilon^2/2)$ and $\Delta = \epsilon^2$. To resolve possible ambiguities, we insist that the twist operator is the ground state of the twisted sector. This means that we take $\epsilon \in \left[-\frac{1}{2}, \frac{1}{2}\right]$. Let us call σ_l the twist operator in the lth copy that implements a twist by $e^{2\pi i m_l}$. The full twist operator is

$$\mathcal{T}_{n,\gamma} = \prod_{l=1}^{n} \sigma_l = \prod_{l=1}^{n} e^{i m_l \tilde{\varphi}_l} \tag{C6}$$

[21] This computation is adapted from Section 2.4 of [62]. The minus signs in the second line are due to the fact that we are dealing with fermions, as in thermal partition functions, as explained in Section 2 of [63].

[22] Take $S = (1/8\pi) \int d^2\sigma\, \partial_\mu \varphi \partial^\mu \varphi$ with $\varphi \cong \varphi + 2\pi R$. The operators $\mathcal{O}_{n,w} = e^{in\varphi/R} e^{iwR\tilde{\varphi}/2}$ (where the dual scalar $\tilde{\varphi}$ is defined by $\partial_\mu \tilde{\varphi} = \epsilon_{\mu\nu} \partial^\nu \varphi$) have conformal dimensions and spin

$$h_{n,w} = \frac{1}{2}\left(\frac{n}{R} + \frac{wR}{2}\right)^2, \qquad \bar{h}_{n,w} = \frac{1}{2}\left(\frac{n}{R} - \frac{wR}{2}\right)^2, \qquad \Delta_{n,w} = \frac{n^2}{R^2} + \frac{w^2 R^2}{4}, \qquad s_{n,w} = nw.$$

T-duality maps $R \leftrightarrow 2/R$. The case $R = 1$ gives the bosonization of the Dirac fermion. Indeed, $\mathcal{O}_{1/2,1} = \tilde{\psi}_L$ and $\mathcal{O}_{-1/2,-1} = \tilde{\psi}_L^\dagger$ are the left-moving fermions while $\mathcal{O}_{1/2,-1} = \tilde{\psi}_R$ and $\mathcal{O}_{-1/2,1} = \tilde{\psi}_R^\dagger$ are the right-moving fermions.

Downloaded from https://academic.oup.com/ptep/article/2025/6/063B05/8140051 by SISSA - Scuola Internazionale Superiore di Studi Avanzati user on 15 June 2026

and its conformal dimension is

$$\Delta[\mathcal{T}_{n,\gamma}] = \sum_{l=1}^{n} m_l^2 = \frac{n^2-1}{12n}. \tag{C7}$$

This reproduces the dimension of the twist fields in the case of central charge $c = 1$ [34] and shows that such a dimension does not depend on the parameters γ_k [17].

Let us now compute the Renyi asymmetries of the coherent states created by V for a finite subset $A = [-\ell, \ell]$ as in Section 4.1. For simplicity, we take the insertions along the imaginary axis: $w_- = -i\eta$ and $w_+ = i\eta$. The correlator we need to compute is thus

$$\mathcal{A} = \left\langle \mathcal{T}_{n,\gamma}(-\ell)\mathcal{T}_{n,\gamma}^{\dagger}(\ell)\left(\prod_{j=1}^{n} e^{i\lambda V_j(-i\eta)}\right)\left(\prod_{j=1}^{n} e^{-i\lambda V_j^{\dagger}(i\eta)}\right)\right\rangle_{\mathcal{S}^{(n)},\mathbb{C}}. \tag{C8}$$

Here V_j is the primary in the jth copy, and we put identical insertions in each copy. In Eq. (C1) there is one such correlator in the numerator integrated over $\vec{\gamma}$, and one such correlator in the denominator with $\vec{\gamma} = 0$. We expand the correlator in λ. At zeroth order we have

$$\mathcal{A}^{(0)} = \langle \mathcal{T}_{n,\gamma}(-\ell)\mathcal{T}_{n,\gamma}^{\dagger}(\ell)\rangle = \frac{1}{(2\ell)^{2\Delta_{\mathcal{T}}}}, \tag{C9}$$

where $\Delta_{\mathcal{T}} = (n^2-1)/12n$. At second order we have

$$\mathcal{A}^{(2)} = \left\langle \mathcal{T}_{n,\gamma}\mathcal{T}_{n,\gamma}^{\dagger} \sum_{k_1,k_2}(V_{k_1}V_{k_2}^{\dagger})\right\rangle, \tag{C10}$$

where we have left the dependence on positions implicit to ease the notation. We expand each of the fields in the diagonalizing basis:[23] the twist operators are as in Eq. (C6), while

$$\begin{aligned} V_{k_1} &= \frac{1}{n}\sum_{j_1,j_2} \exp\left(\frac{2\pi i}{n}(j_1+j_2-n-1)k_1 - 2i\alpha_{k_1}\right)\tilde{\psi}_{Lj_1}\tilde{\psi}_{Rj_2}, \\ V_{k_2}^{\dagger} &= \frac{1}{n}\sum_{j_3,j_4} \exp\left(-\frac{2\pi i}{n}(j_3+j_4-n-1)k_2 + 2i\alpha_{k_2}\right)\tilde{\psi}_{Lj_3}^{\dagger}\tilde{\psi}_{Rj_4}^{\dagger}. \end{aligned} \tag{C11}$$

When we substitute in correlator (C10), we obtain six sums. However, if we insert $\tilde{\psi}_{Lj_1}$ then there must also be $\tilde{\psi}_{Lj_1}^{\dagger}$ or else the correlator vanishes, which means that we restrict to $j_3 = j_1$. Similarly, we restrict to $j_4 = j_2$. We thus find that

$$\begin{aligned} \mathcal{A}^{(2)} = \frac{1}{n^2}\sum_{k_1,k_2,j_1,j_2} &\exp\left[\frac{2\pi i}{n}(j_1+j_2-n-1)(k_1-k_2) - 2i(\alpha_{k_1}-\alpha_{k_2})\right] \\ &\times\left\langle\left(\prod_{l} e^{im_l\tilde{\varphi}_l}e^{-im_l\tilde{\varphi}_l}\right)\tilde{\psi}_{Lj_1}\tilde{\psi}_{Rj_2}\tilde{\psi}_{Lj_1}^{\dagger}\tilde{\psi}_{Rj_2}^{\dagger}\right\rangle. \end{aligned} \tag{C12}$$

In the numerator the integrals over $\vec{\gamma}$, equivalent to integrals over $\vec{\alpha}$, impose $k_1 = k_2$. In the denominator there are no such integrals. So, at order λ^2, we are left with a sum over $k_1 \neq k_2$ (and no α's). We need to compute each term of this sum.

To compute the correlators, we use the Coulomb gas formalism, i.e. we separately compute the left- and right-moving contributions. The holomorphic part of a correlator is

$$\langle e^{i\epsilon_1\varphi_L}(z_1)\cdots e^{i\epsilon_n\varphi_L}(z_n)\rangle = \prod_{i<j}^{n}(z_i - z_j)^{\epsilon_i\epsilon_j}. \tag{C13}$$

[23] The inverse to Eq. (C3) is $\Psi_k = (1/\sqrt{n})\sum_{l=1}^{n}\exp[2\pi i(2l-n-1)k/2n - i\alpha_k]\tilde{\Psi}_l$.

Downloaded from https://academic.oup.com/ptep/article/2025/6/063B05/8140051 by SISSA - Scuola Internazionale Superiore di Studi Avanzati user on 15 June 2026

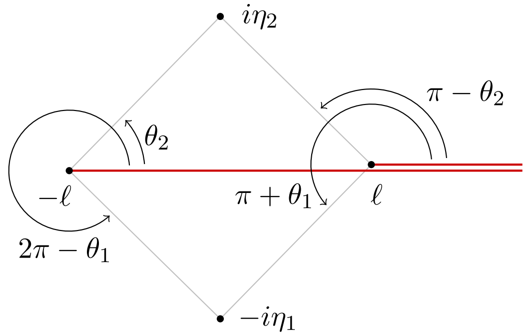

Fig. C1. Phases involved in the four-point function $\langle e^{i\epsilon\varphi_L}(-\ell)e^{-i\epsilon\varphi_L}(\ell)e^{i\varphi_L}(-i\eta_1)e^{-i\varphi_L}(i\eta_2)\rangle$.

The left-moving part of the correlator is given by

$$\begin{aligned}\mathcal{A}^{(2)}_{L,k_1k_2} &= \frac{1}{n}\sum_{j_1=1}^{n}\left\langle\left(\prod_l e^{im_l\varphi_{Ll}}(-\ell)e^{-im_l\varphi_{Ll}}(\ell)\right)e^{i\varphi_{Lj_1}}(-i\eta)e^{-i\varphi_{Lj_1}}(i\eta)\right\rangle e^{2\pi i(2j_1-n-1)(k_1-k_2)/2n}\\ &= \left(\prod_{l\neq j_1}(2\ell)^{-m_l^2}\right)\frac{1}{n}\sum_{j_1=1}^{n}\frac{(2\ell)^{-m_{j_1}^2}}{2i\eta}\left[\frac{(i\eta-\ell)(-i\eta+\ell)}{(i\eta+\ell)(-i\eta-\ell)}\right]^{m_{j_1}}e^{2\pi i(2j_1-n-1)(k_1-k_2)/2n}\\ &= \frac{n^{-1}}{(2\ell)^{\Delta_T}(2i\eta)}\sum_{j_1=1}^{n}e^{2\pi i(2j_1-n-1)(k_1-k_2+\tau_0/\pi)/2n}\\ &= \frac{1}{(2\ell)^{\Delta_T}(2i\eta)}\frac{\sin[\pi(k_1-k_2)+\tau_0]}{n\sin\{[\pi(k_1-k_2)+\tau_0]/n\}},\end{aligned} \tag{C14}$$

where $\tau_0 = 2\arctan(\ell/\eta)$. To correctly evaluate the second line, we placed the cut of each twist operator on the right, and this unambiguously fixes all phases. In particular,

$$\begin{aligned}\langle e^{i\epsilon\varphi_L}(-\ell)e^{-i\epsilon\varphi_L}(\ell)e^{i\varphi_L}(-i\eta_1)e^{-i\varphi_L}(i\eta_2)\rangle &= \frac{1}{(2\ell)^{\epsilon^2}i(\eta_1+\eta_2)}\frac{(i\eta_2-\ell)^{\epsilon}(-i\eta_1+\ell)^{\epsilon}}{(i\eta_2+\ell)^{\epsilon}(-i\eta_1-\ell)^{\epsilon}}\\ &= \frac{1}{(2\ell)^{\epsilon^2}i(\eta_1+\eta_2)}\frac{e^{i(\pi-\theta_2)\epsilon}e^{i(2\pi-\theta_1)\epsilon}}{e^{i\theta_2\epsilon}e^{i(\pi+\theta_1)}}\\ &= \frac{1}{(2\ell)^{\epsilon^2}i(\eta_1+\eta_2)}e^{i(2\pi-2\theta_1-2\theta_2)\epsilon},\end{aligned} \tag{C15}$$

where $\tan\theta_j = \eta_j/\ell$ and $0<\theta_j<\pi/2$. Here it is important that all angles are taken from the cut (towards the right) going counterclockwise. See Fig. C1. In our example we take $\theta_1=\theta_2\equiv\theta$ and, defining $\tan(\tau_0/2)=\ell/\eta$, we have $\theta=(\pi-\tau_0)/2$.

The right-moving part of the correlator is similar, however: $\varphi_{Lj}\to\varphi_{Rj}$; the twist operator is $e^{-i\epsilon\varphi_R}$; all dependencies are on the antiholomorphic coordinates. This is the same as mapping $\epsilon\to-\epsilon$ and $\eta\to-\eta$, and it gives

$$\mathcal{A}^{(2)}_{R,k_1k_2} = \frac{1}{(2\ell)^{\Delta_T}(-2i\eta)}\frac{\sin[\pi(k_1-k_2)+\tau_0]}{n\sin\{[\pi(k_1-k_2)+\tau_0]/n\}}. \tag{C16}$$

Putting the two contributions together, we find that

$$\mathcal{A}^{(2)}_{k_1k_2} = \frac{1}{(2\ell)^{2\Delta_T}4\eta^2}\frac{\sin^2(\tau_0)}{n^2\sin^2\{[\pi(k_1-k_2)+\tau_0]/n\}}. \tag{C17}$$

Downloaded from https://academic.oup.com/ptep/article/2025/6/063B05/8140051 by SISSA - Scuola Internazionale Superiore di Studi Avanzati user on 15 June 2026

The expansion of Eq. (C1) in λ gives

$$\begin{aligned}\Delta S_n &= \frac{1}{1-n}\log\frac{\mathcal{A}^{(0)}+\lambda^2[1/(2\pi)^n]\int d\vec{\alpha}\,\sum_{k_1k_2}\mathcal{A}^{(2)}_{k_1k_2}(\vec{\alpha})+O(\lambda^4)}{\mathcal{A}^{(0)}+\lambda^2\sum_{k_1k_2}\mathcal{A}^{(2)}_{k_1k_2}(0)+O(\lambda^4)}\\ &= \frac{1}{1-n}\log\frac{1+(\lambda^2/\mathcal{A}^{(0)})\sum_k\mathcal{A}^{(2)}_{kk}+O(\lambda^4)}{1+(\lambda^2/\mathcal{A}^{(0)})\sum_{k_1k_2}\mathcal{A}^{(2)}_{k_1k_2}+O(\lambda^4)}\\ &= \frac{\lambda^2}{n-1}\sum_{k_1\neq k_2}^{n}\frac{\mathcal{A}^{(2)}_{k_1k_2}}{\mathcal{A}^{(0)}}+O(\lambda^4).\end{aligned} \tag{C18}$$

The sum over $k_1 \neq k_2$ is essentially the same one that we already encountered in Eq. (A1) for $\Delta = 1$. Therefore, at quadratic order,

$$\Delta S_n^{(2)} = \frac{1}{n-1}\frac{1}{4\eta^2}\left(n-\frac{\sin^2(\tau_0)}{n\sin^2(\tau_0/n)}\right). \tag{C19}$$

This is indeed the Renyi asymmetry of an interval in the case $\Delta = 1$ that one obtains by performing a conformal transformation from the Rindler geometry and using Eq. (30). The limit $n \to 1$ gives $\Delta S^{(2)}_{\text{disk}} = [1-\tau_0\cot(\tau_0)]/2\eta^2$ that reproduces Eq. (60).

Appendix D. Embedding formalism

In Poincaré coordinates, the metric of Euclidean AdS$_{d+1}$ is

$$ds^2 = \frac{dz^2+dx_1^2+\cdots+dx_d^2}{z^2}, \tag{D1}$$

where $z > 0$. This can be obtained from the embedding formalism by introducing constrained coordinates $P_A = (P_{-1}, P_0, \ldots, P_d)$ that satisfy

$$P\cdot P \equiv -P_{-1}^2+P_0^2+\sum\nolimits_{i=1}^d P_i^2 = -1, \qquad P_{-1}\geq 1, \tag{D2}$$

and projecting the flat metric $ds^2 = -dP_{-1}^2+dP_0^2+\sum_{i=1}^d dP_i^2$. This displays the SO$(d+1,1)$ isometry. The Poincaré coordinates are obtained from the parametrization

$$P_{-1} = \frac{1+z^2+\vec{x}^2}{2z}, \qquad P_0 = \frac{1-z^2-\vec{x}^2}{2z}, \qquad P_{i=1,\ldots,d} = \frac{x_i}{z}. \tag{D3}$$

Here $\vec{x} = (x_i) = (x_1, \ldots, x_d)$. The conformal boundary is at $z = 0$.

The Rindler coordinates appearing in Eq. (98) are obtained from the parametrization

$$P_{-1} = \rho Y_0, \quad P_0 = \sqrt{\rho^2-1}\cos(\tau), \quad P_d = \sqrt{\rho^2-1}\sin(\tau), \quad P_{a=1,\ldots,d-1} = \rho Y_a, \tag{D4}$$

where $\rho \geq 1$, the variable $\tau \in [0, 2\pi)$ is an angle, while (Y_0, Y_a) are auxiliary coordinates on $\mathbb{H}^{d-1}$ that satisfy $-Y_0^2+\sum_{a=1}^{d-1}Y_a^2 = -1$ and $Y_0 \geq 1$. We parametrize them as

$$Y_0 = \cosh(u), \qquad Y_{a=1,\ldots,d-1} = \sinh(u)\theta_a, \tag{D5}$$

where $u \geq 0$ (although in the case of $d = 2$ we could set $\theta_1 = 1$ and use $u \in \mathbb{R}$), while θ_a satisfy $\sum_{a=1}^{d-1}\theta_a^2 = 1$ and describe a sphere S^{d-2} of radius 1. The induced metric is Eq. (98), i.e.

$$ds^2 = (\rho^2-1)\,d\tau^2+\frac{d\rho^2}{\rho^2-1}+\rho^2[du^2+\sinh^2(u)\,d\Omega_{d-2}^2], \tag{D6}$$

where $d\Omega_{d-2}^2$ is the metric on S^{d-2} induced from $ds^2 = \sum_a d\theta_a^2$. The two parametrizations of P_A given above define the change of coordinates.

Downloaded from https://academic.oup.com/ptep/article/2025/6/063B05/8140051 by SISSA - Scuola Internazionale Superiore di Studi Avanzati user on 15 June 2026

In Poincaré coordinates the bulk-to-boundary propagator is as in Eq. (93):

$$K_E(z, \vec{x} \mid \vec{x}') = C_\Delta \left(\frac{z}{z^2 + (\vec{x} - \vec{x}')^2} \right)^\Delta . \tag{D7}$$

In order to derive the propagator in Rindler coordinates, we use the identity

$$\begin{aligned} -2\rho Y \cdot Y' - 2\sqrt{\rho^2 - 1}\cos(\tau - \tau') &= 2[P_{-1} Y_0' - P_0 \cos(\tau') - P_a Y_a' - P_d \sin(\tau')] \\ &= [Y_0' + \cos(\tau')] \frac{z^2 + (\vec{x} - \vec{x}')^2}{z}, \end{aligned} \tag{D8}$$

where[24]

$$x_a' = \frac{Y_a'}{Y_0' + \cos(\tau')}, \qquad x_d' = \frac{\sin(\tau')}{Y_0' + \cos(\tau')}, \qquad \vec{x}'^2 = \frac{Y_0' - \cos(\tau')}{Y_0' + \cos(\tau')}. \tag{D9}$$

The primed coordinates identify a point on the conformal boundary. In Poincaré coordinates, the metric induced on the conformal boundary at $z = 0$ from Eq. (D1) is the flat one of $\mathbb{R}^d$, namely, $ds_\partial^2 = d\vec{x}'^2$. In these coordinates we regard x_d' as the Euclidean time, and consider the spherical spatial subregion $A = \{x_d' = 0,\ \vec{x}'^2 < 1\}$ where the second term indicates the Euclidean norm of the spatial coordinates. The change of boundary coordinates (D9) gives

$$ds_\partial^2 = d\vec{x}'^2 = \Omega^{-2}[d\tau'^2 + du'^2 + \sinh^2(u')\, d\Omega_{d-2}'^2], \qquad \Omega = \cosh(u') + \cos(\tau') . \tag{D10}$$

Here Ω is precisely the conformal factor (97), also appearing in Eq. (D8). The metric in parentheses is that of $S^1 \times \mathbb{H}^{d-1}$, which is also the metric on the conformal boundary at $\rho = \infty$ induced from Eq. (D6). The spherical spatial subregion A is mapped to a copy of $\mathbb{H}^{d-1}$ at $\tau' = 0$. Since the propagator transforms as a primary of dimension Δ, using Eq. (D8), we conclude that

$$K_E(\rho, \tau, Y \mid \tau', Y') = \frac{C_\Delta}{[-2\rho Y \cdot Y' - 2\sqrt{\rho^2 - 1}\cos(\tau - \tau')]^\Delta}. \tag{D11}$$

References

[1] A. C. Wall, Phys. Rev. D **85**, 104049 (2012); **87**, 069904 (2013) [erratum] [arXiv:1105.3445 [gr-qc]] [Search inSPIRE].

[2] H. Casini and M. Huerta, Phys. Rev. D **85**, 125016 (2012), [arXiv:1202.5650 [hep-th]] [Search inSPIRE].

[3] T. Faulkner, R. G. Leigh, O. Parrikar, and H. Wang, J. High. Energy Phys. **09**, 038 (2016), [arXiv:1605.08072 [hep-th]] [Search inSPIRE].

[4] T. Faulkner, M. Guica, T. Hartman, R. C. Myers, and M. Van Raamsdonk, J. High. Energy Phys. **03**, 051 (2014), [arXiv:1312.7856 [hep-th]] [Search inSPIRE].

[5] A. Almheiri, X. Dong, and D. Harlow, J. High. Energy Phys. **04**, 163 (2015), [arXiv:1411.7041 [hep-th]] [Search inSPIRE].

[6] G. Penington, J. High. Energy Phys. **09**, 002 (2020), [arXiv:1905.08255 [hep-th]] [Search inSPIRE].

[7] A. Almheiri, N. Engelhardt, D. Marolf, and H. Maxfield, J. High. Energy Phys. **12**, 063 (2019), [arXiv:1905.08762 [hep-th]] [Search inSPIRE].

[8] J. de Boer, V. Godet, J. Kastikainen, and E. Keski-Vakkuri, J. High. Energy Phys. **09**, 087 (2023), [arXiv:2306.00099 [hep-th]] [Search inSPIRE].

[9] F. Ares, S. Murciano, and P. Calabrese, Nat. Commun. **14**, 2036 (2023), [arXiv:2207.14693 [cond-mat.stat-mech]] [Search inSPIRE].

[10] E. B. Mpemba and D. G. Osborne, Phys. Educ. **4**, 172 (1969).

[24] To invert these formulas (we omit primes), one can use $x_d = \sin(\tau)/[Y_0 + \cos(\tau)]$, $(1 - \vec{x}^2)/2 = \cos(\tau)/[Y_0 + \cos(\tau)]$, from which one extracts $\tan(\tau) = 2x_d/(1 - \vec{x}^2)$ and $Y_0 = (1 + \vec{x}^2)/\sqrt{(1 - \vec{x}^2)^2 + 4x_d^2} \geq 1$.

Downloaded from https://academic.oup.com/ptep/article/2025/6/063B05/8140051 by SISSA - Scuola Internazionale Superiore di Studi Avanzati user on 15 June 2026

[11] Z. Lu and O. Raz, Proc. Natl. Acad. Sci. U.S.A. **114**, 5083 (2017), [arXiv:1609.05271 [cond-mat.stat-mech]] [Search inSPIRE].
[12] A. Kumar and J. Bechhoefer, Nature **584**, 64 (2020), [arXiv:2008.02373 [cond-mat.stat-mech]] [Search inSPIRE].
[13] L. Kh. Joshi et al., Phys. Rev. Lett. **133**, 010402 (2024), [arXiv:2401.04270 [quant-ph]] [Search inSPIRE].
[14] F. Ares, S. Murciano, E. Vernier, and P. Calabrese, SciPost Phys. **15**, 089 (2023), [arXiv:2302.03330 [cond-mat.stat-mech]] [Search inSPIRE].
[15] B. Bertini, K. Klobas, M. Collura, P. Calabrese, and C. Rylands, Phys. Rev. B **109**, 184312 (2024), [arXiv:2306.12404 [cond-mat.stat-mech]] [Search inSPIRE].
[16] F. Ferro, F. Ares, and P. Calabrese, J. Stat. Mech., **02**, 023101 (2024), [arXiv:2307.06902 [cond-mat.stat-mech]] [Search inSPIRE].
[17] L. Capizzi and M. Mazzoni, J. High. Energy Phys. **12**, 144 (2023), [arXiv:2307.12127 [cond-mat.stat-mech]] [Search inSPIRE].
[18] L. Capizzi and V. Vitale, J. Phys. A: Math. Theor. **57**, 45LT01 (2024), [arXiv:2310.01962 [quant-ph]] [Search inSPIRE].
[19] C. Rylands, K. Klobas, F. Ares, P. Calabrese, S. Murciano, and B. Bertini, Phys. Rev. Lett. **133**, 010401 (2024), [arXiv:2310.04419 [cond-mat.stat-mech]] [Search inSPIRE].
[20] S. Murciano, F. Ares, I. Klich, and P. Calabrese, J. Stat. Mech. **01**, 013103 (2024), [arXiv:2310.07513 [cond-mat.stat-mech]] [Search inSPIRE].
[21] M. Chen and H.-H. Chen, Phys. Rev. D **109**, 065009 (2024), [arXiv:2310.15480 [hep-th]] [Search inSPIRE].
[22] F. Caceffo, S. Murciano, and V. Alba, J. Stat. Mech. **06**, 063103 (2024), [arXiv:2402.02918 [cond-mat.stat-mech]] [Search inSPIRE].
[23] M. Fossati, F. Ares, J. Dubail, and P. Calabrese, J. High. Energy Phys. **05**, 059 (2024), [arXiv:2402.03446 [hep-th]] [Search inSPIRE].
[24] S. Yamashika, F. Ares, and P. Calabrese, Phys. Rev. B **110**, 085126 (2024), [arXiv:2403.04486 [cond-mat.stat-mech]] [Search inSPIRE].
[25] S. Liu, H.-K. Zhang, S. Yin, and S.-X. Zhang, Phys. Rev. Lett. **133**, 140405 (2024), [arXiv:2403.08459 [quant-ph]] [Search inSPIRE].
[26] K. Chalas, F. Ares, C. Rylands, and P. Calabrese, J. Stat. Mech. 103101 (2024), [arXiv:2405.04436 [cond-mat.stat-mech]] [Search inSPIRE.
[27] F. Ares, V. Vitale, and S. Murciano, Phys. Rev. B **111**, 104312 (2025), [arXiv:2405.08913 [cond-mat.stat-mech]] [Search inSPIRE].
[28] X. Turkeshi, P. Calabrese, and A. De Luca, arXiv:2405.14514 [quant-ph] [Search inSPIRE].
[29] K. Klobas, C. Rylands, and B. Bertini, Phys. Rev. B **111**, L140304 (2025) [arXiv:2406.04296 [cond-mat.stat-mech]] [Search inSPIRE].
[30] M. Botta-Cantcheff, P. Martínez, and G. A. Silva, J. High. Energy Phys. **02**, 171 (2016), [arXiv:1512.07850 [hep-th]] [Search inSPIRE].
[31] A. Christodoulou and K. Skenderis, J. High. Energy Phys. **04**, 096 (2016), [arXiv:1602.02039 [hep-th]] [Search inSPIRE].
[32] T. Faulkner, F. M. Haehl, E. Hijano, O. Parrikar, C. Rabideau, and M. Van Raamsdonk, J. High. Energy Phys. **08**, 057 (2017), [arXiv:1705.03026 [hep-th]] [Search inSPIRE].
[33] C. Holzhey, F. Larsen, and F. Wilczek, Nucl. Phys. B **424**, 443 (1994), [arXiv:hep-th/9403108] [Search inSPIRE].
[34] P. Calabrese and J. L. Cardy, J. Stat. Mech. **0406**, P06002 (2004), [arXiv:hep-th/0405152] [Search inSPIRE].
[35] P. Calabrese and J. Cardy, J. Phys. A **42**, 504005 (2009), [arXiv:0905.4013 [cond-mat.stat-mech]] [Search inSPIRE].
[36] N. Lashkari and M. Van Raamsdonk, J. High. Energy Phys. **04**, 153 (2016), [arXiv:1508.00897 [hep-th]] [Search inSPIRE].
[37] J. Cardy and E. Tonni, J. Stat. Mech. **1612**, 123103 (2016), [arXiv:1608.01283 [cond-mat.stat-mech]] [Search inSPIRE].
[38] P. Calabrese and J. L. Cardy, Phys. Rev. Lett. **96**, 136801 (2006), [arXiv:cond-mat/0601225] [Search inSPIRE].

Downloaded from https://academic.oup.com/ptep/article/2025/6/063B05/8140051 by SISSA - Scuola Internazionale Superiore di Studi Avanzati user on 15 June 2026

[39] Z. Ma, C. Han, Y. Meir, and E. Sela, Phys. Rev. A **105**, 042416 (2022), [arXiv:2110.09388 [quant-ph]] [Search inSPIRE].
[40] N. Laflorencie and S. Rachel, J. Stat. Mech. **11**, P11013 (2014), [arXiv:1407.3779 [cond-mat.str-el]] [Search inSPIRE].
[41] M. Goldstein and E. Sela, Phys. Rev. Lett. **120**, 200602 (2018), [arXiv:1711.09418 [cond-mat.stat-mech]] [Search inSPIRE].
[42] J. C. Xavier, F. C. Alcaraz, and G. Sierra, Phys. Rev. B **98**, 041106 (2018), [arXiv:1804.06357 [cond-mat.stat-mech]] [Search inSPIRE].
[43] D. Gaiotto, A. Kapustin, N. Seiberg, and B. Willett, J. High. Energy Phys. **02**, 172 (2015), [arXiv:1412.5148 [hep-th]] [Search inSPIRE].
[44] M. Gutperle, Y.-Y. Li, D. Rathore, and K. Roumpedakis, J. High Energy Phys. **09**, 010 (2024), [arXiv:2406.10967 [hep-th]] [Search inSPIRE].
[45] J. Cardy, Phys. Rev. Lett. **112**, 220401 (2014), [arXiv:1403.3040 [cond-mat.stat-mech]] [Search in SPIRE].
[46] J. M. Maldacena, Adv. Theor. Math. Phys. **2**, 231 (1998), [arXiv:hep-th/9711200] [Search inSPIRE].
[47] S. S. Gubser, I. R. Klebanov, and A. M. Polyakov, Phys. Lett. B **428**, 105 (1998), [arXiv:hep-th/9802109] [Search inSPIRE].
[48] E. Witten, Adv. Theor. Math. Phys. **2**, 253 (1998), [arXiv:hep-th/9802150] [Search inSPIRE].
[49] S. Ryu and T. Takayanagi, Phys. Rev. Lett. **96**, 181602 (2006), [arXiv:hep-th/0603001] [Search in SPIRE].
[50] A. Lewkowycz and J. Maldacena, J. High. Energy Phys. **08**, 090 (2013), [arXiv:1304.4926 [hep-th]] [Search inSPIRE].
[51] G. Penington, S. H. Shenker, D. Stanford, and Z. Yang, J. High. Energy Phys. **03**, 205 (2022), [arXiv:1911.11977 [hep-th]] [Search inSPIRE].
[52] A. Almheiri, T. Hartman, J. Maldacena, E. Shaghoulian, and A. Tajdini, J. High. Energy Phys. **05**, 013 (2020), [arXiv:1911.12333 [hep-th]] [Search inSPIRE].
[53] D. Z. Freedman, S. D. Mathur, A. Matusis, and L. Rastelli, Nucl. Phys. B **546**, 96 (1999), [arXiv:hep-th/9804058] [Search inSPIRE].
[54] H. Casini, M. Huerta, and R. C. Myers, J. High. Energy Phys. **05**, 036 (2011), [arXiv:1102.0440 [hep-th]] [Search inSPIRE].
[55] S. Hollands and R. M. Wald, Commun. Math. Phys. **321**, 629 (2013), [arXiv:1201.0463 [gr-qc]] [Search inSPIRE].
[56] N. Lashkari, J. Lin, H. Ooguri, B. Stoica, and M. Van Raamsdonk, Prog. Theor. Exp. Phys. **12**, 12C109 (2016), [arXiv:1605.01075 [hep-th]] [Search inSPIRE].
[57] A. May and E. Hijano, J. High. Energy Phys. **10**, 036 (2018), [arXiv:1806.06077 [hep-th]] [Search inSPIRE].
[58] J. Lee and R. M. Wald, J. Math. Phys. **31**, 725 (1990).
[59] R. M. Wald, Phys. Rev. D **48**, R3427 (1993), [arXiv:gr-qc/9307038] [Search inSPIRE].
[60] V. Iyer and R. M. Wald, Phys. Rev. D **50**, 846 (1994), [arXiv:gr-qc/9403028] [Search inSPIRE].
[61] G. E. Andrews, R. Askey, and R. Roy, *Special Functions, Encyclopedia of Mathematics and Its Applications* (Cambridge University Press, Cambridge, 1999).
[62] A. Belin, L.-Y. Hung, A. Maloney, S. Matsuura, R. C. Myers, and T. Sierens, J. High. Energy Phys. **12**, 059 (2013), [arXiv:1310.4180 [hep-th]] [Search inSPIRE].
[63] H. Casini, C. D. Fosco, and M. Huerta, J. Stat. Mech. **0507**, P07007 (2005), [arXiv:cond-mat/0505563] [Search inSPIRE].

Downloaded from https://academic.oup.com/ptep/article/2025/6/063B05/8140051 by SISSA - Scuola Internazionale Superiore di Studi Avanzati user on 15 June 2026

© The Author(s) 2025. Published by Oxford University Press on behalf of the Physical Society of Japan.
This is an Open Access article distributed under the terms of the Creative Commons Attribution License (https://creativecommons.org/licenses/by/4.0/), which permits unrestricted reuse, distribution, and reproduction in any medium, provided the original work is properly cited.
Funded by SCOAP[3]